

# **Technoeconomic Analysis of Perovskite Photovoltaic Manufacturing for Powering Telecommunications Towers**

by

Justin Xiao

S.B., Massachusetts Institute of Technology (2017)

Submitted to the Department of Electrical Engineering and Computer  
Science

in partial fulfillment of the requirements for the degree of

Master of Engineering in Electrical Engineering and Computer Science

at the

**MASSACHUSETTS INSTITUTE OF TECHNOLOGY**

June 2018

© Massachusetts Institute of Technology 2018. All rights reserved.

Author .....  
Department of Electrical Engineering and Computer Science  
May 25, 2018

Certified by .....  
Vladimir Bulović  
Professor of Electrical Engineering and Computer Science  
Thesis Supervisor

Accepted by .....  
Katriona LaCurts  
Chair, Master of Engineering Thesis Committee



# **Technoeconomic Analysis of Perovskite Photovoltaic Manufacturing for Powering Telecommunications Towers**

by

Justin Xiao

Submitted to the Department of Electrical Engineering and Computer Science  
on May 25, 2018, in partial fulfillment of the  
requirements for the degree of  
Master of Engineering in Electrical Engineering and Computer Science

## **Abstract**

In recent years, metal halide perovskite solar cells have gained traction as a potential competitor to the mature silicon-based solar cells in terms of both cost and performance. Being a young technology, however, means little is known about its true market value. In order to understand this, it is important to both get an accurate estimate of manufacturing cost and explore potential applications.

In this thesis, we develop a Monte Carlo cost analysis method and apply it towards a realistic perovskite module manufacturing sequence today. We determine a nominal cost estimate of \$101.7/m<sup>2</sup>, which for a 15% efficient module comes out to \$0.68/W. Compared to silicon, which hovers around \$0.40/W, this is rather competitive, since most of the installed system cost comes from non-module components such as installation labor and racking.

With the lightweight and flexible form factor of perovskite solar modules, new applications become possible. One such application is the installation of perovskite photovoltaics (PV) vertically on telecommunications towers. Since such towers cannot support the weight of conventional silicon PV, this is a potential market for perovskite PV that silicon cannot satisfy. Using HOMER microgrid simulation software, we determine that it is financially feasible to install vertical PV in countries with high diesel prices and low grid reliability, such as India.

Thesis Supervisor: Vladimir Bulović  
Title: Professor of Electrical Engineering and Computer Science



## Acknowledgments

I would like to thank my advisor Vladimir Bulović, ONE Lab, and GridEdge for providing such a lovely environment for me to finish my M. Eng. I can't possibly imagine a more warm and welcoming environment, and Vladimir's good-natured cheerfulness inspires those around him to reach for their potential. The chance to work as a part of GridEdge was everything I could have asked for.

To Joel Jean, whose contributions to this thesis are immeasurable, I cannot express enough gratitude. Joel's leadership and wealth of knowledge on all things solar are unparalleled. Whenever I talk to him, I feel like I learn something and am re-energized to do the best work I can. But more than that, Joel is an outstanding human - rarely will you meet someone as caring. He somehow always knows the right things to say, and during the various trials and tribulations over the year I knew Joel was rooting for me. Joel will remain the gold standard to which I aspire for many years to come.

I am immensely grateful for Ryan Zimmerman, whose expertise in mechanical engineering has been crucial for this thesis. I could not have asked for a better partner on this project.

I want to thank Sanjay Aggarwal, Jason Hirsch, and Ed Knapp from ATC. Because of our collaboration, I had the opportunity to work on something interesting and meaningful. Even more, their boundless enthusiasm and support have made working with them an absolute pleasure.

I thank my friends in Next Two East, the best living group I could have asked for. My roommates at SBE, Framien Koko, Paul Reynolds and Brenda Stein, are the most wonderful group of friends to come home to. I will miss bonding over our mutual struggles through M. Eng-ing over boba (which we had to get delivered ourselves). I'm sorry for every time I did my chores late.

A final round of thanks - to my parents, whose bottomless support has given me all the strength I've needed to get to where I am today. Tina, whose moving to Boston has been one of the single best things to happen to me this year. I will miss our coffee talks. And Alissa, to whom I wish good luck on the next banner.



# Contents

<b>1</b>	<b>Introduction</b>	<b>13</b>
1.1	Introduction to Solar Energy . . . . .	14
1.2	Introduction to Photovoltaics . . . . .	15
1.2.1	Physics of Solar Cells . . . . .	15
1.2.2	Circuit Model of Solar Cells . . . . .	16
1.2.3	Solar Cell Efficiency . . . . .	17
1.3	Basics of Perovskite Photovoltaics . . . . .	20
1.4	Economics of Perovskite Photovoltaics . . . . .	22
<b>2</b>	<b>Module Manufacturing Cost Modeling</b>	<b>23</b>
2.1	Cost Modeling Approaches . . . . .	23
2.1.1	Bottom-up Spreadsheet Cost Modeling . . . . .	23
2.1.2	Monte Carlo Cost Modeling . . . . .	24
2.2	Cost Modeling Methodology . . . . .	25
2.2.1	Factory Assumptions . . . . .	26
2.2.2	Material Cost . . . . .	26
2.2.3	Tool Cost . . . . .	27
2.2.4	Monte Carlo modeling of Costs . . . . .	31
2.3	Defining a Manufacturing Sequence . . . . .	36
2.3.1	Single Junction Perovskite Reference Module and Manufacturing Sequence . . . . .	37
2.4	Cost Model Results . . . . .	38
2.5	Discussion . . . . .	42

2.6 Chapter Acknowledgements . . . . .	45
<b>3 Economics of Vertically Deployed Photovoltaics on Telecommunications Towers</b>	<b>47</b>
3.1 Telecommunications Towers: A Background . . . . .	47
3.2 Wind Loading on Telecommunications Towers with PV . . . . .	49
3.3 HOMER Microgrid Simulation . . . . .	52
3.3.1 Defining Our HOMER Model . . . . .	52
3.4 Simulating Tower Microgrids in Nigeria . . . . .	54
3.4.1 HOMER Results . . . . .	55
3.4.2 Is Vertical PV Financially Viable in Nigeria? . . . . .	58
3.5 Simulating Tower Microgrids in India . . . . .	58
3.5.1 HOMER Results . . . . .	59
3.5.2 Is Vertical PV Financially Viable in India? . . . . .	62
3.6 Chapter Acknowledgements . . . . .	63
<b>4 Conclusions and Future Work</b>	<b>65</b>
<b>A Cost Model Inputs</b>	<b>67</b>
A.1 Materials Inputs . . . . .	67
A.2 Tools Inputs . . . . .	68
A.3 Factory Assumptions . . . . .	69

# List of Figures

1-1	Global PV market share by technology in 2013 . . . . .	14
1-2	Equivalent circuit model of solar cell. . . . .	17
1-3	$I - V$ curve for a solar cell. The open-circuit voltage $V_{oc}$ , short-circuit current $I_{sc}$ , fill factor $FF$ , and maximum power point $MPP$ are labeled.	18
1-4	Efficiency records for various solar cell technologies over time as of 2018. Courtesy of NREL. . . . .	19
1-5	Basic perovskite structure, courtesy of Eames et al.[10]	20
2-1	Probability distributions for (a) $X$ , (b) $Y$ , and the (c) Monte Carlo results for $Z$ in our Monte Carlo toy model. The results of trial $i$ are highlighted. . . . .	33
2-2	Visualization of beta-PERT distribution. The distribution goes to zero at the endpoints, and increasing lambda makes the peak larger and narrower. . . . .	36
2-3	Perovskite solar cell structure . . . . .	37
2-4	Diagram of roll-to-roll manufacturing sequence for perovskite solar modules . . . . .	38
2-5	Manufacturing cost distribution in $\$/m^2$ . . . . .	39
2-6	Manufacturing cost distribution in $\$/W$ . . . . .	39
2-7	The 5 most costly components of the given manufacturing sequence in $\$/m^2$ . Error bars indicate the 10th and 90th percentile estimates for each component's cost. . . . .	40

2-8	Manufacturing sequence cost breakdown by process in \$/m <sup>2</sup> , broken down by materials cost, capex, labor, opex and cost associated with yield loss. . . . .	41
2-9	Normalized uncertainty of materials costs . . . . .	42
2-10	Normalized uncertainty of tools costs . . . . .	43
2-11	Sputterer depreciation cost as a function. This assumes a \$6.5M sputterer in a factory operating 3690 hours a year with a depreciation period of 7 years. . . . .	44
3-1	Deflection of tower under maximum wind load with no PV . . . . .	50
3-2	Linear regression to find the maximum allowed PV area . . . . .	51
3-3	Schematic of HOMER inputs . . . . .	52
3-4	Heat map of optimal PV installation size (1 kWp minimum) with varying PV cost and diesel cost in Maiduguri, Nigeria. . . . .	56
3-5	Heat map of change in net present cost given the PV installation in Figure 3-4 with varying PV cost and diesel cost in Maiduguri, Nigeria. . . . .	56
3-6	Heat map of renewable fraction given the PV installation in Figure 3-4 with varying PV cost and diesel cost in Maiduguri, Nigeria. . . . .	57
3-7	Heat map of change in diesel usage reduction given the PV installation in Figure 3-4 with varying PV cost and diesel cost in Maiduguri, Nigeria. . . . .	57
3-8	Heat map of optimal PV installation size (1 kWp minimum) with varying PV cost and grid reliability in Rajasthan, India. . . . .	60
3-9	Heat map of change in net present cost given the PV installation in Figure 3-8 with varying PV cost and grid reliability in Rajasthan, India. . . . .	60
3-10	Heat map of renewable fraction given the PV installation in Figure 3-8 with varying PV cost and grid reliability in Rajasthan, India. . . . .	61
3-11	Heat map of change in diesel usage reduction given the PV installation in Figure 3-8 with varying PV cost and grid reliability in Rajasthan, India. . . . .	61

# List of Tables

2.1	Factory assumptions . . . . .	26
2.2	Materials cost input parameters . . . . .	27
2.3	Tool cost input parameters . . . . .	28
2.4	Cost distribution results, assuming a 15% module efficiency . . . . .	40
3.1	Wind force on different panel geometries . . . . .	51
3.2	Base assumptions for key Nigeria microgrid simulation inputs . . . . .	55
A.1	Cost model materials inputs . . . . .	67
A.2	Tool cost inputs, where tool cost ( $\$M$ ) is the total upfront cost of the tool, facility cost (% of tool cost) is the cost of support services such as air or chemical delivery, floor space ( $m^2$ ) is the footprint of the tool itself, spare parts (% capex/yr) is any replacement parts that the tool needs every year, and electricity usage (kW) is the power demand of the tool. . . . .	68
A.3	Tool cost inputs, where throughput is the area process in an hour of operation ( $m^2/hr$ ), downtime is the percentage of time the tool is maintained instead of operating (% of time), operation staff is the number of operators needed to operate the tool, maintenance staff is the number of staff needed to conduct maintenance or repair, and yield is the percentage of modules process that are good (%). . . . .	68

A.4 Factory assumptions, where the electricity cost is the local cost of grid electricity, electricity for services is the ratio of electricity for services/tool electricity, floor space ratio is the ratio of total factory floor space/tool footprint, building cost is the cost of building a factory, operator labor rate is the wage for operators, maintenance technician labor rate is the technician wage, indirect labor cost ratio is the ratio of indirect labor/direct labor (set to 0 here because it is accounted for in later steps), facilities and equipment depreciation times are the depreciation times for all facilities and tools respectively, and number of operating hours is the hours per year the factory operates. . . . . 69

# Chapter 1

## Introduction

In today's society, environmental issues have been increasingly brought to the forefront of the public consciousness, all around the world. A 2016 Pew Research Center survey found that 74% of U.S adults believe that "the country should do whatever it takes to protect the environment."<sup>[6]</sup> Despite being the largest emitter of greenhouse gases, China aims to spend \$360 billion on renewable energy through 2020 and is already the world's largest investor in renewable energy<sup>[11]</sup>. This environmentalism on China's part results largely from an attempt to curb deadly air pollution in many of its cities, as well as an awareness that its coastal cities face an existential threat in rising sea levels.

Partly due to growing concerns about climate change, the renewable energy industry has boomed. The International Energy Agency (IEA) predicts a 43% growth on today's total installed renewable energy capacity by 2022. Among renewable energy resources, solar is dominating. In 2016, installed photovoltaic (PV) capacity surpassed coal additions for the first time. This is driven by an abundance of solar resource as well as continuously decreasing costs<sup>[5]</sup>.

In the current PV market, conventional crystalline silicon (c-Si) is the dominant force. By 2013, the global PV market was 90% c-Si PV, with less than 10% thin-film solar cells<sup>[14]</sup>. However, with the emergence of new PV technologies, in particular metal halide perovskites, it appears that c-Si may have a challenger. Perovskite thin-film PV shows the potential to reach a lower \$/W cost than c-Si, which would allow

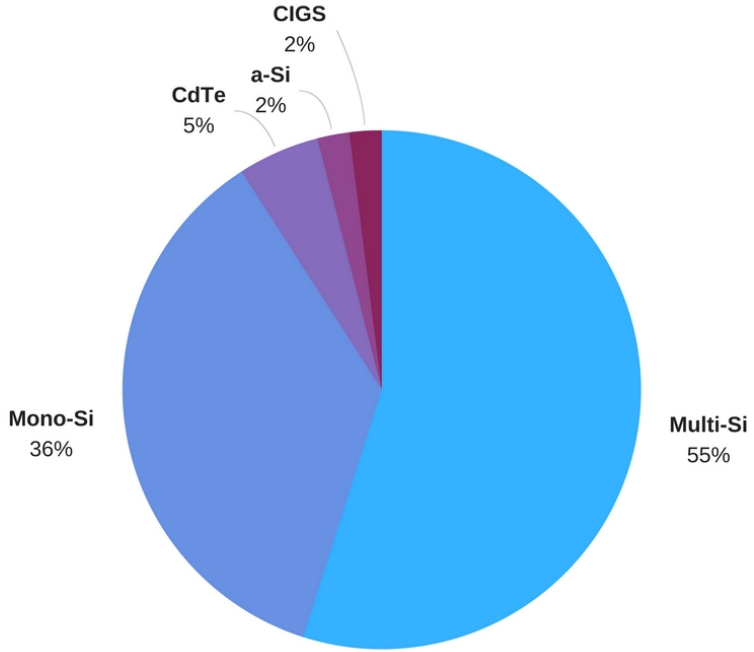


Figure 1-1: Global PV market share by technology in 2013

it to achieve wider market penetration.

In Chapter 1, we discuss the basics of solar energy, photovoltaics, as well as perovskite PV. In Chapter 2, we discuss the importance of manufacturing cost modeling, our methodology for finding a reliable cost estimate, and cost-modeling results. Chapter 3 applies these costs to a potential application: powering telecommunications towers. Finally, Chapter 4 provides a future path for this work and summarizes the thesis.

## 1.1 Introduction to Solar Energy

The sun provides nearly all useable energy on Earth, whether directly (capturing the sun's rays for heat or power) or indirectly (such as through fossil fuels, which is essentially stored solar energy captured by plants millions of years ago). Intuitively, we would assume the sun thus supplies a very large amount of energy to the Earth on a daily basis. Indeed, the solar power incident on the Earth's surface at any

time is approximately  $1.73 \times 10^{17}$  W. To put this into perspective, the 2014 energy consumption was 155,481 TWh, which translates to an average global consumption rate of  $1.78 \times 10^{13}$  W. We see that the sun provides us a tremendous amount of power!

We can model the sun as a black-body radiation source with temperature 5,778 K in order to understand its radiation composition. From Stefan-Boltzmann's law, we can calculate that the sun produces  $P_{\text{sun}} = A\sigma T_{\text{sun}}^4 = 3.85 \times 10^{26}$  W. Since the photon flux must be constant, an inverse-square law applies to the energy that reaches the surface, so we receive a solar constant of 1.381 kW/m<sup>2</sup> at the top of Earth's atmosphere under AM0 (air mass 0, i.e. no atmosphere). At the Earth's surface, and we see a power density reduction from AM0 across the solar spectrum due to light passing through air molecules and dust. Additionally, different molecules (O<sub>2</sub>, N<sub>2</sub>, CO<sub>2</sub>, etc.) have different absorption peaks, where they strongly absorb light at particular wavelengths. This manifests in power density dips at certain frequency bands within the solar spectrum. The typical spectrum used for rating and testing terrestrial solar modules is AM1.5 (1.5 atmospheres thick on average).

## 1.2 Introduction to Photovoltaics

Solar energy can be collected for human use in multiple formats. The two more well known methods are solar-to-thermal and solar-to-electrical energy. In solar-to-thermal, solar energy is collected to heat an element (often water) for various purposes, such as cooking or steam to power turbines. The method that this thesis focuses on is photovoltaics, which converts light directly into electricity.

### 1.2.1 Physics of Solar Cells

Any discussion on photovoltaics begins with the physics of semiconductors. Consider a classical semiconductor with two energy bands: the valence band and the conduction band, separated by a forbidden energy bandgap ( $E_g$ ). In an intrinsic (undoped) semiconductor at 0 K, the valence band is completely filled with electrons, and the conduction band is completely empty. No free charge carriers are present, and thus

no electrical current flows under an applied electric field. At higher temperatures, a small number of electrons are excited from the valence band to the conduction band, leaving behind positively-charged holes in the valence band. Both types of free carriers—electrons in the conduction band and holes in the valence band—can move freely and thus contribute to current flow. Similarly, in a semiconductor doped with a small number of atoms with a different valence from the prevailing species (e.g., boron or phosphorus for silicon), excess electrons or holes—in an n-type or p-type semiconductor, respectively—are available for conduction.

A solar cell consists of a p-n junction, where a p-type semiconductor is joined with an n-type semiconductor. This combination creates a built-in potential difference across the junction. When an incident photon with energy greater than  $E_g$  is absorbed, it excites an electron from the valence band to the conduction band, creating an excess photogenerated electron-hole pair. If the electron or hole is sufficiently close to the depletion region, the built-in electric field sweeps it across the junction, thus separating the electron and hole. If the junction is connected externally, the majority carrier flows through the external circuit until it meets the minority carrier in the junction and recombines. This creates a net light-induced current flow.

### 1.2.2 Circuit Model of Solar Cells

We now discuss the circuit model of a solar cell. Since an ideal solar cell is simply a current-generating p-n junction, the ideal solar cell circuit model would be a current source in parallel with a diode. However, a real solar cell has parasitic resistances that affect its efficiency. This can be represented by adding a parallel shunt resistance, as well as a series resistance. The final equivalent circuit is shown in Figure 1-2. Here,  $I_L$  represents the photo-generated current,  $I_d$  is the current that flows through the diode,  $I_{sh}$  is the current through the shunt resistance  $R_{sh}$  and  $R_s$  is the series resistance.

There are three important parameters that describe the efficiency of a solar cell: open-circuit voltage ( $V_{oc}$ ), short-circuit current ( $I_{sc}$ ), and fill factor ( $FF$ ).  $V_{oc}$  is the maximum possible voltage measured across the cell, which is when there is an open

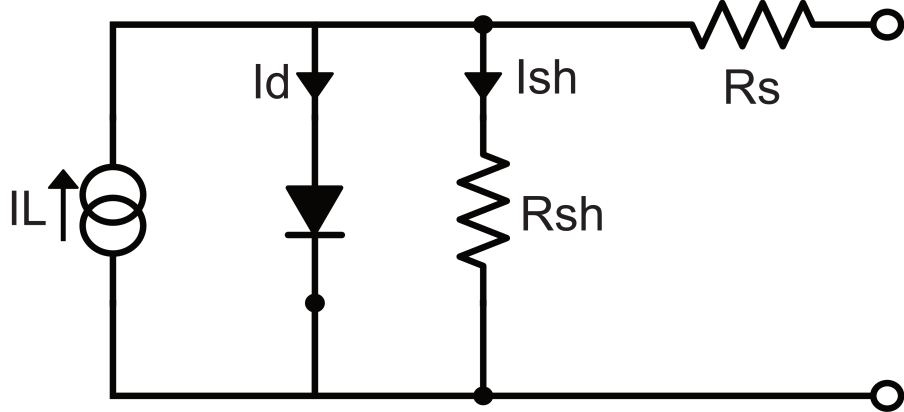


Figure 1-2: Equivalent circuit model of solar cell.

load across it. This voltage can be calculated as

$$V_{oc} = \frac{n k_B T}{q} \ln \left( \frac{I_L}{I_0} + 1 \right)$$

where  $n$  is some diode ideality factor,  $I_0$  is saturation current, and  $q$  is elementary charge. At open-circuit, no current flows across the device.

$I_{sc}$  is a measure of the maximum current that can flow through the solar cell, which occurs when the leads are shorted together. It is approximately the same as the photo-generated current,  $I_{sc} = I_L$ . At short-circuit, there is no voltage across the device.

### 1.2.3 Solar Cell Efficiency

At open-circuit and short-circuit conditions, it is impossible to extract power from the solar cell (since power  $P = VI$ ). Instead, there is a maximum power point ( $MPP$ ) on the solar cell  $I - V$  curve, at which the most amount of power possible is drawn from the cell. The fill factor  $FF$  can be calculated as

$$FF = \frac{V_{MPP} \times I_{MPP}}{V_{oc} I_{sc}}$$

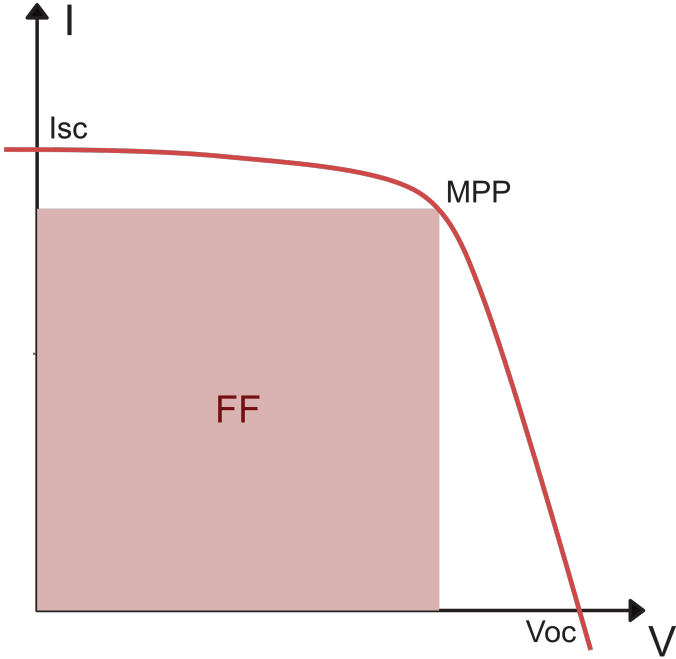


Figure 1-3:  $I - V$  curve for a solar cell. The open-circuit voltage  $V_{oc}$ , short-circuit current  $I_{sc}$ , fill factor  $FF$ , and maximum power point  $MPP$  are labeled.

where  $V_{MPP}$  is the voltage at  $MPP$  and  $I_{MPP}$  is the current at  $MPP$ . This is illustrated in Figure 1-3.

From these parameters we can calculate the power conversion efficiency ( $PCE$ ) of a solar cell. This efficiency tells us, given some incident power, how much power the device can output. It is calculated simply as

$$PCE = \frac{V_{oc} I_{sc} FF}{P_{in}}$$

where  $P_{in}$  is the incident solar power. Thus, we want to maximize the  $V_{oc}$ ,  $I_{sc}$  and  $FF$  for a more efficient cell.

In 1961, William Shockley and Hans-Joachim Quiesser calculated the so-called Shockley-Quiesser limit[21], which puts an upper bound on the maximum possible  $PCE$  attainable by a single-junction p-n type solar cell. Assuming AM1.5 conditions, this limit occurs for a material with a 1.34 eV bandgap, achieving a  $PCE$  of 33.7%. For silicon, with an indirect bandgap of 1.1 eV, the limit is 29.4%. Now, the limit

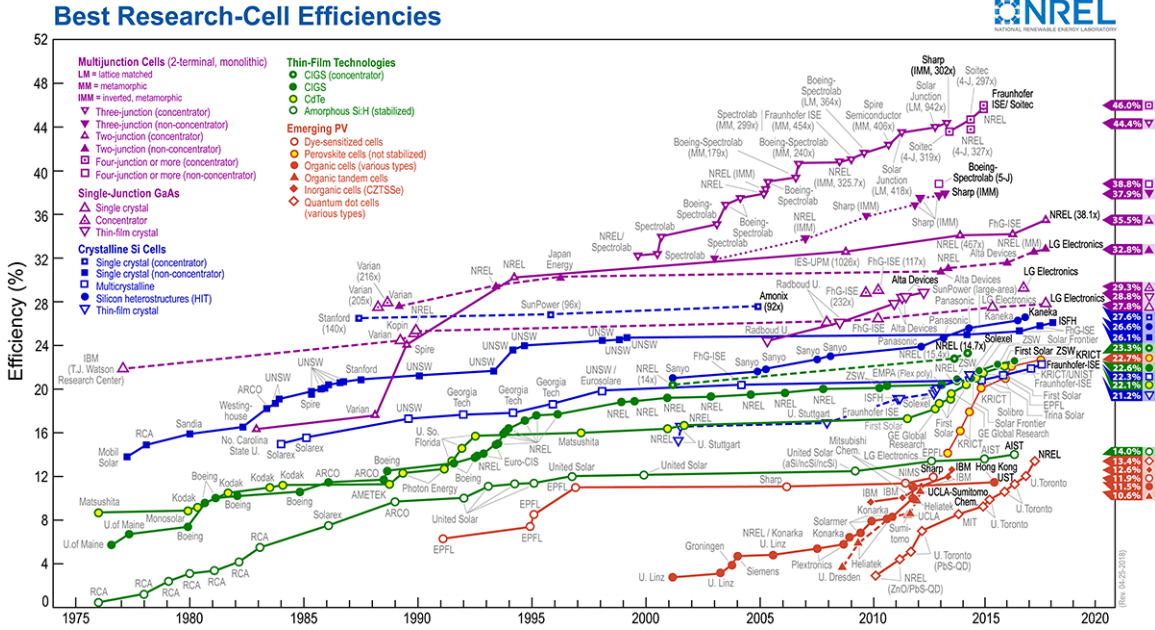


Figure 1-4: Efficiency records for various solar cell technologies over time as of 2018. Courtesy of NREL.

can be exceeded in a variety of ways, including with multi-junction cells or solar concentration. However, we shall focus on single-junction cells for the majority of this work.

An important question to ask is: how close we can get to this limit? After all, the limit is only for an ideal cell, and ignores losses due to parasitic resistances, light reflection from the top of the cell, light blockage due to interconnections, and other such practical matters. We can start by looking at the record efficiency for various solar cell technologies over time. The National Renewable Energy Laboratory (NREL) has compiled this data and has made a popular graph depicting it, as reproduced in Figure 1-4.

We can infer a lot of information from this figure. For instance, the current record efficiency for a single-junction silicon cell without the use of a concentrator sits at 26.6%[29]. However, more interesting (in the opinion of the author) is the meteoric rise of perovskite cells. First demonstrated in 2009 with an efficiency of merely 3.9%, perovskite solar cells have managed to skyrocket in record efficiency to 22.7% by 2017[16], in the span of 8 years. We focus in this thesis on perovskite solar PV, with

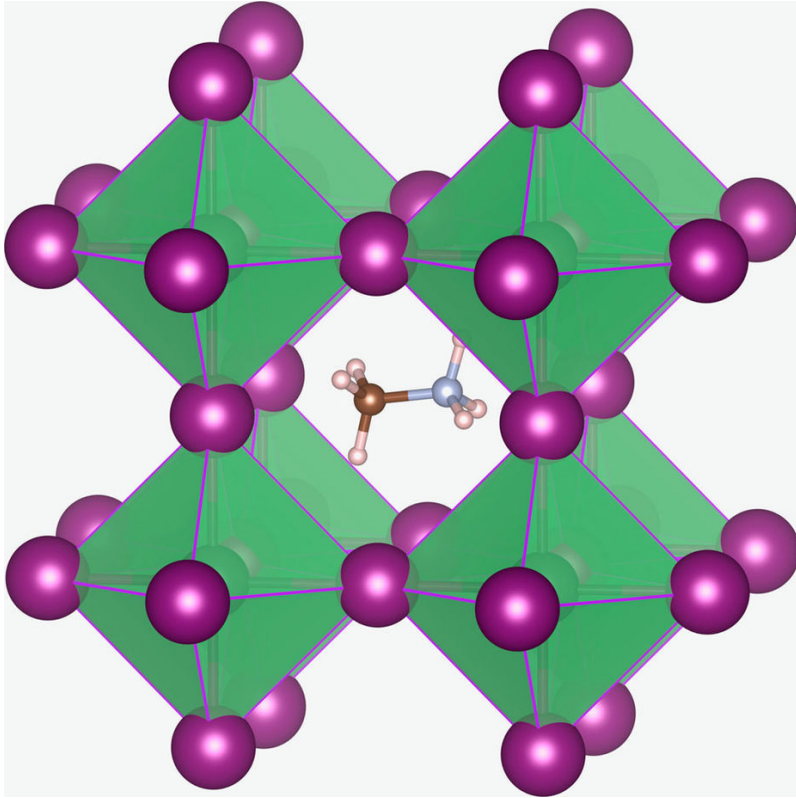


Figure 1-5: Basic perovskite structure, courtesy of Eames et al.[10]

the aim of determining the technoeconomic feasibility of introducing perovskite PV into the market.

### 1.3 Basics of Perovskite Photovoltaics

In this section we explore the fundamental characteristics of perovskite solar cells. As the name implies, these solar cells use compounds with the perovskite crystal structure as the light-absorbing material in the active layer. Perovskites have an  $\text{ABX}_3$  structure, in which A and B are cations (with A larger than B), and X is an anion that binds to both. The structure is shown in Figure 1-5.

One of the most common perovskites used for photovoltaics is methylammonium lead trihalide ( $\text{MAPbX}_3$ ), with X = I, Br, or Cl. By altering the halide content the bandgap of the perovskite can be tuned and thus optimized for absorption of light from the sun[27].

There are multiple physical factors that contribute to the promising performance of perovskite solar cells. For one, perovskites have a high dielectric constant. If a photon with high enough energy is incident upon the perovskite, an electron-hole bound pair called an exciton is formed. Since the exciton binding energy depends on the Coulomb interaction between an electron and hole, which is inversely proportional to the dielectric constant, this means that the exciton binding energy is low. Indeed, this binding energy has been measured to be as low as <5 meV[9][22]. Since room temperature thermal energy is at 25 meV, these excitons disassociate into free electrons and holes very easily, allowing for improved charge collection.

In addition, charge carriers in perovskites can travel over one micron. This is due to the unique properties of defects in perovskites. In typical semiconductors, defects such as lattice site vacancies or interstitial ions introduce energy levels in the middle of the bandgap, such that when charge carriers meet the defect they fall into those energy levels and lose energy or recombine. This reduces the charge carrier density and thus photocurrent. However, perovskites have the interesting property where point defects introduce energy bands near the edge of the conduction/valence bands, so recombination is mitigated and perovskites maintain high conductivity in thin-film formats[28].

One of the chief advantages of perovskites is their simplicity of processing. While c-Si solar cells require high-temperature processes, perovskites can be made with simple, low-temperature, and easily scalable deposition techniques. It has also been demonstrated that ink-jet printing perovskites is a viable option[20]. This enables roll-to-roll processing of perovskite solar cells, similar to the way newspapers are printed. This could potentially simplify and reduce costs of perovskite solar cell manufacturing.

The simpler and cheaper processing, the requirement for less material in thin-film formats, and the continued rise in efficiency make perovskite PV a very attractive candidate. However, in order to be truly competitive, perovskites must eventually be cheaper than c-Si PV. Currently, commercial silicon module production cost sits at around \$0.40/W[19] and is dropping. A new PV technology can only be economically

viable if it can be produced and sold at a similar, cheap price. It is thus very important to estimate the manufacturing cost of a perovskite solar cell module if we want to predict its scalability and marketability.

## 1.4 Economics of Perovskite Photovoltaics

In recent years, there has been some effort towards pinning down a cost estimate of manufacturing perovskite solar modules. For example, Chang et al. estimated a cost of \$107/m<sup>2</sup> in 2017 for perovskite-on-glass modules[8]. In comparison, depending on *PCE*, a typical silicon PV module costs between \$60/m<sup>2</sup> - \$100/m<sup>2</sup> to manufacture. While Chang's estimate seems high, in this 2017 paper they assumed very costly materials such as Au and Ag, impractical manufacturing sequences, as well as slow-throughput deposition techniques. Later in 2017, Song et al. proposed a much more optimistic cost estimate of \$31.7/m<sup>2</sup>[25].

In these papers, the manufacturing sequence was designed to produce rigid perovskite-on-glass modules. However, one of the exciting prospects of perovskite PV is its potential for a lightweight, flexible form factor. This allows for potential roll-to-roll (R2R) manufacturing, which could potentially reduce capital costs dramatically. In 2018, Chang et al. estimated a \$37/m<sup>2</sup> manufacturing cost using a R2R manufacturing sequence[7].

For this thesis, we develop a cost model based on Chang's approach. We then examine a perovskite R2R manufacturing sequence and obtain our own cost estimates.

In the search for potential markets for perovskite PV, we apply our cost estimate to determine the economic feasibility of powering telecommunications towers. We use the microgrid simulation tool HOMER, using our cost estimates as well as data provided by ATC as inputs. In the next two chapters, we go over our methodology for our modeling, as well as the results.

# Chapter 2

## Module Manufacturing Cost Modeling

When deciding whether it is worth scaling up production of a technology, it is of utmost importance to get a reliable estimate of the final cost of manufacturing. After all, one can not simply invest the capital to build a factory only to find that the final product is prohibitively expensive. For a technology as young as perovskite PV, it becomes even more important to get an accurate estimate, especially when competing with such a cheap and mature competitor like silicon.

In this chapter, we discuss our methodology towards getting a cost estimate. We will talk about what has been done already towards this effort, as well as what our cost model does differently. We will then define a manufacturing sequence and generate cost estimates given this sequence.

### 2.1 Cost Modeling Approaches

#### 2.1.1 Bottom-up Spreadsheet Cost Modeling

One of the most widely cited approaches to cost modeling for perovskites comes from Song's 2017 paper[25], which draws heavily from the spreadsheet approach of Powell et al. in their c-Si cost model[18]. In their approach, they first define a reference

module. In the paper the module was assumed to be a p-i-n structure of  $\text{MAPbI}_3$  between NiO and ZnO, respectively. Additionally, it was assumed that the module would be sandwiched between glass plates to prevent degradation.

Once the module is defined, it becomes possible to define a manufacturing sequence. In particular, Song chose to use screen printing of the charge transport and perovskite layers due to its low cost.

A manufacturing sequence can be divided into a series of processes, where each process is typically centered around a tool. For example, ITO sputtering would be centered around a sputtering tool. The final cost estimate can be calculated by summing the costs associated with each process. The final module cost is given by the equation

$$MC = \sum_i (M_i + U_i + L_i + E_i + D_i)$$

where  $M_i$  is the materials cost for process  $i$ ,  $U_i$  is the utilities cost,  $L_i$  is the labor cost,  $E_i$  is the equipment maintenance cost and  $D_i$  is the equipment and building depreciation cost.

Song found that the final module cost was  $\$31.7 \pm 5.5/\text{m}^2$ .  $\$6.8 \pm 1.2/\text{m}^2$  is associated with the processing of the cells, while  $\$24.9 \pm 4.3/\text{m}^2$  is for the materials. This is a very low cost, which suggests a very favorable path forward for perovskite manufacturing.

While Song's approach provides good insight, it is difficult to include uncertainty in the analysis. When doing a spreadsheet calculation, one typically performs the calculation with precise definitions for the input values, which makes it difficult to calculate outputs based on a spread of values.

### 2.1.2 Monte Carlo Cost Modeling

In a different approach to cost modeling employed by Chang[8][7], one gets cost estimates using probability distributions for each input by employing a Monte Carlo approach. This is a common method in financial analyses, as it is difficult to predict cost values with precision. In a Monte Carlo approach, a probability distribution

is defined for each parameter. The model then samples from each distribution and calculates the final cost using these samples, building a final cost distribution by repeating this process for a large number of trials.

The Monte Carlo method has an advantage over the spreadsheet-based approach in that it very easily incorporates uncertainty into the analysis. This is very applicable to perovskite PV manufacturing, since the technology is still in its early stages and many of the parameters determining cost are uncertain.

In Chang’s Monte Carlo analysis of R2R perovskite PV[7], it was found that demonstrated R2R manufacturing processes can achieve costs of  $\$60/m^2 \pm 30\%$ , while an optimized but difficult to realize process could be as low as  $\$37/m^2 \pm 30\%$ . While these numbers are promising, they appear to be optimistic. Most crucially, Chang assumes an unrealistically cheap barrier layer. This is not likely to be realistic.

In our approach to cost modeling, we have built on top of Chang’s methodology. Using our cost model, we defined a manufacturing sequence we believe to be realistic and obtained a cost distribution. In addition, we hoped to make cost modeling a flexible and simple process, so that as inputs become more refined it remains easy to run cost modeling. In this vein, we created a Python library and Jupyter notebook template that makes the cost modeling process simple.

## 2.2 Cost Modeling Methodology

In this section we will go over the cost modeling methodology, starting from how the inputs are defined and the equations used for calculating cost. We then review the Monte Carlo process. The first step in calculating the total manufacturing cost is the definition of a manufacturing sequence. This sequence is broken down as a series of processes. For each process, there are two type of cost components: materials cost and tools/facilities cost. First, we define a set of factory assumptions.

### 2.2.1 Factory Assumptions

The factory assumptions are important factors associated with the factory itself that play into how cost is calculated. For example, the amount spent on labor is determined by the wage in the area that the factory is located, and the amount spent on electricity is determined by the cost of electricity in the area. The full set of factory assumptions is defined in Table 2.1 below.

<i>Abbreviation</i>	<i>Parameter</i>	<i>Units</i>	<i>Description</i>
<i>BC</i>	Building cost	\$/m <sup>2</sup>	Building cost
<i>EC</i>	Electricity cost	\$/kWh	Cost of electricity
<i>ES</i>	Electricity for services	Ratio	Ratio of electricity for services to electricity for tools
<i>FSR</i>	Floor space ratio	Ratio	Ratio of total factory space to tool footprint
<i>OL</i>	Operator labor rate	\$/hr	Labor rate for operators
<i>ML</i>	Maintenance technician labor rate	\$/hr	Labor rate for maintenance technicians
<i>IL</i>	Indirect labor cost ratio	Ratio	Ratio of indirect to direct labor
<i>FD</i>	Facilities depreciation period	yr	Depreciation period of facilities
<i>ED</i>	Equipment depreciation period	yr	Depreciation period of tools
<i>OH</i>	Number of operating hours	hr/yr	Hours in year that factory operates
<i>PCE</i>	Cell PCE	%	Cell active area power conversion efficiency
<i>GFF</i>	Geometric fill factor	Ratio	Fractional area of active power conversion on module

Table 2.1: Factory assumptions

### 2.2.2 Material Cost

#### Material Cost Parameters

Materials cost is defined as the cost of raw materials that go into manufacturing the product. Typically, the materials cost will dominate the total manufacturing cost for mature, high-throughput processes. In order to calculate materials cost, we provide two inputs: material usage and material cost. These are summarized in Table 2.2 below.

<i>Abbreviation</i>	<i>Parameter</i>	<i>Units</i>	<i>Description</i>
<i>MU</i>	Material usage	unit/m <sup>2</sup>	The amount of material used in one square meter of module
<i>MC</i>	Material cost	\$/unit	Cost per unit of the material

Table 2.2: Materials cost input parameters

### Material Cost Calculation

In order to calculate the contribution of raw materials to the cost of each process, we use Equation 2.1.

$$M = MU \times MC \quad (2.1)$$

For a thin-film process, we calculate the material usage as

$$MU = \frac{\rho \times t}{u}$$

where  $\rho$  is the density of the material,  $t$  is the thickness of the stack layer that the material applies to, and  $u$  is the percentage of the material utilized. We see that, to determine materials cost, one essentially only needs to know the amount of material that is used for an area of the module, as well as the cost of purchasing some amount of the material.

### 2.2.3 Tool Cost

#### Tool Cost Parameters

The tool cost for each process can be thought of as the cost of purchasing and running the tool used in that process. In order to calculate the contribution of the tool to the final cost, we provide a set of parameters summarized in Table 2.3 below.

#### Tool Cost Calculation

The most obvious tool cost contribution is that of tool depreciation cost. This is the capital expenditure (capex) associated with purchasing the tool. This cost is

Abbreviation	Parameter	Units	Description
<i>TC</i>	Tool cost	\$M	Total upfront cost of the tool
<i>FC</i>	Facility cost	% of tool cost	Cost of services for the tool
<i>FS</i>	Floor space	m <sup>2</sup>	Tool footprint
<i>SP</i>	Spare parts	% of capex/year	Cost of spare parts for the tool
<i>EU</i>	Electricity usage	kW	Power consumption of the tool
<i>TP</i>	Throughput	m <sup>2</sup> /hr	Module area produced in one hour
<i>DT</i>	Down time	% of time	Percentage of time that tool is maintained
<i>OS</i>	Operation staff	Number of staff	Staff that operate the tool
<i>MS</i>	Maintenance staff	Number of staff	Staff that maintain the tool
<i>Y</i>	Yield	% of good parts produced	Percentage of parts that are good out of all produced

Table 2.3: Tool cost input parameters

allocated over an amount of time known as the depreciation period. In our model, we assume a linear depreciation such that the depreciation cost is distributed evenly across the depreciation period. The tool depreciation cost can be calculated as

$$T = \frac{TC}{TP \times OH \times ED} \quad (2.2)$$

Another contribution to the tool cost is the facilities cost. This is a capex cost associated with the facilities for a given tool. Facilities, defined here, are the services associated with operating a tool, air (such as chemical delivery, N<sub>2</sub>, compressed or dry air), or water. It is assumed that the more expensive the tool, the more must be spent on such services, so the facilities cost is given as a percentage of the tool cost, except with a different depreciation period set by the facilities depreciation period rather than the equipment depreciation period. Thus, facilities depreciation cost can be calculated as

$$F = \frac{T \times FC \times ED}{FD} \quad (2.3)$$

The final contribution to capex comes from building depreciation. This is the depreciation cost associated with building a factory of a given size. The factory size is determined by the total tool footprint. The amount of floor space for a given tool footprint is determined by the floor space ratio. From the total floor space, the cost of building the factory can be determined. This building cost is given in Equation 2.4

$$B = \frac{FS \times FSR \times BC}{TP \times OH \times FD} \quad (2.4)$$

The labor cost is dependent on the number of workers as well as the wage. There are two types of labor: operation staff and maintenance staff. The operation staff is responsible for running the tool when it is operational. However, if the tool is down or needs maintenance, the maintenance staff is responsible for fixing the tool. The ratio of time in maintenance mode vs. the time in operation mode is given by the tool's downtime  $DT$ . We expect operation staff to have different wages than maintenance staff, due to the difference in specialization. Thus, we add the operational staff cost  $OSC$  and maintenance staff cost  $MSC$  to find the labor cost. Additionally, there is some indirect labor contributions from workers such as custodial or office work, so we include an indirect labor ratio  $IL$ . We thus calculate labor costs as follows:

$$\begin{aligned} OSC &= \frac{OS \times OL \times (1 - DT)}{TP} \\ MSC &= \frac{MS \times ML \times DT}{TP} \\ L &= (OSC + MSC) \times (1 + IL) \end{aligned} \tag{2.5}$$

Finally, we calculate the operational expenses (opex). This is the cost associated with running the factory, and includes electricity costs as well as spare parts for machinery and facilities. We calculate the cost for electricity  $E$ , which depends on the local electricity rate  $EC$  as well as the amount of power  $EU$  required to run the tool. In addition, there is a cost associated with powering services, such as lighting and air conditioning, which we assume to be proportional to the tool electricity usage so we include an electricity for services ratio  $ES$ . For spare parts, we assume that the cost spent on spare parts  $SPC$  is proportional to the capex by some percentage  $SP$ . We can thus calculate the total opex as

$$\begin{aligned} E &= \frac{EC \times EU \times (1 + ES)}{TP} \\ SPC &= (T + F + B) \times SP \\ O &= E + SPC \end{aligned} \tag{2.6}$$

For all parameters so far, we use similar definitions as in the 2017 paper by Chang et al.[8]

## **Yield**

The manufacturing process is not ideal, and each process will not produce 100% good parts. To take this into account, we add a yield parameter for each tool which defines the percentage of good parts produced. Calculating the impact of yield on cost is somewhat complex. If a process produces a bad module, then all of the cost invested into the previous processes for that module is wasted. Thus, the yield loss for a particular process incorporates the loss aggregated over all previous processes.

Consider the  $n$ th process in a sequence with a yield of  $Y_n$ . Before incorporating yield loss, the process has a total cost of  $BYL_n = M_n + T_n + F_n + B_n + L_n + O_n$ . After yield loss is included, the process has a total cost of  $AYL_n$ . Then, when adding the losses from the previous processes, we calculate the yield loss cost  $YC_n$  as

$$YC_n = \left( \frac{BYL_n}{Y_n} - BYL_n \right) + \sum_{i < n} \left( \frac{AYL_i}{Y_n} - AYL_i \right) \quad (2.7)$$

## **Total Manufacturing Cost**

Now that we have defined the cost components, we may talk about the total cost. Similar to both Song and Chang, we calculate the total cost by summing the cost components of each process, and then summing over the processes. Thus, the total manufacturing cost  $C$  is calculated by summing the results from Equations 2.1-2.7. This is given in Equation 2.8.

$$C = \sum_i (M_i + T_i + F_i + B_i + L_i + O_i + YC_i) \quad (2.8)$$

This calculation method lends itself well to a spreadsheet-based bottom-up approach. One just needs to supply a number for every variable for every process and sum to get the final result. However, this requires a large amount of confidence in the numbers supplied, especially for a young technology like perovskite PV. There is very little data on the actual costs of manufacturing this new technology, and it is unreasonable to expect total knowledge of cost parameters and disregard uncertainty. We next talk about how to circumvent this issue using Monte Carlo methods.

## 2.2.4 Monte Carlo modeling of Costs

For any given cost parameter, one would like to incorporate some amount of uncertainty in the calculation. Perhaps the modeler believes the cost parameter to take on some value, but maybe the value can be higher or lower. To incorporate this uncertainty, we use Monte Carlo methods. For every parameter listed in the previous section, the cost modeler defines a nominal estimate - the value they believe to be the most likely. Alongside the nominal estimate, a high estimate is defined that encompasses what the modeler believe to be the highest value the parameter could possibly take, and a low estimate that represents the lowest value the parameter could possibly take.

Once these estimates are defined, we create probability distributions for each parameter. In a single trial, the cost model will sample from each parameter and aggregate them to yield the total cost. The model repeats this process over a large number of trials to form a probability distribution of total cost.

### Monte Carlo: A Toy Model

In this section, we outline a very simple toy model to give some intuition on how the cost model samples and calculates a distribution. Imagine we would like to calculate the probability distribution of values a random variable  $Z$  can take on.  $Z$  is defined as the sum of two other random variables,  $X$  and  $Y$  such that  $Z = X + Y$ . Both  $X$  and  $Y$  take on values defined by a standard normal distribution, so the probability density  $f(x)$  that the random variable  $X$  has a value  $x$  is given by

$$f(x) = \frac{1}{\sqrt{2\pi}} e^{-\frac{x^2}{2}}$$

The random variable  $Y$  is defined similarly.

Let's say that in a given trial, the model samples from  $X$  and  $Y$  according to their probability distributions and adds them. For example, in a single trial  $i$ ,  $X_i = 1.59$  and  $Y_i = -1.32$ , so then  $Z_i = X_i + Y_i = 0.27$ . We repeat these trials many times and plot a histogram of  $Z$  values. This histogram represents a probability distribution for

$Z$ . This is visualized in Figure 2-1.

Now that we have given a cursory understanding of the Monte Carlo model, we may ask what types of probability distributions we should use. We now go over different types of probability distributions, and when they are applicable.

## Uniform distribution

The simplest type of probability distribution is the uniform distribution. It is defined such that, within two bounds  $a$  and  $b$ , all values are equally probable, or

$$f(x) = \begin{cases} \frac{1}{b-a} & \text{for } a \leq x \leq b \\ 0 & \text{for } x < a \text{ or } x > b \end{cases}$$

This is particularly useful if, for some parameter, one only knows a range of values the parameter can take but is unaware of any particular bias. Thus, this distribution is useful for a parameter where the modeller has little knowledge of its value.

## Normal Distribution

One of the most common probability distributions in nature is the normal distribution. This makes it an attractive candidate for modeling the uncertainty of a parameter. This distribution can be parameterized by a mean value  $\mu$ , which is the most likely value for the parameter, as well as a standard deviation  $\sigma$  that represents the spread of possible values. The probability density goes as

$$f(x) = \frac{1}{\sqrt{2\pi}\sigma} e^{-\frac{(x-\mu)^2}{2}}$$

Thus, the modeller can specify a value which they believe to be the most likely for a parameter through  $\mu$ , as well as an uncertainty through  $\sigma$ . In the model, the nominal estimate is defined to be the median, the low estimate is defined to be the 10th percentile of the normal distribution, and the high estimate is set as the 90th percentile.

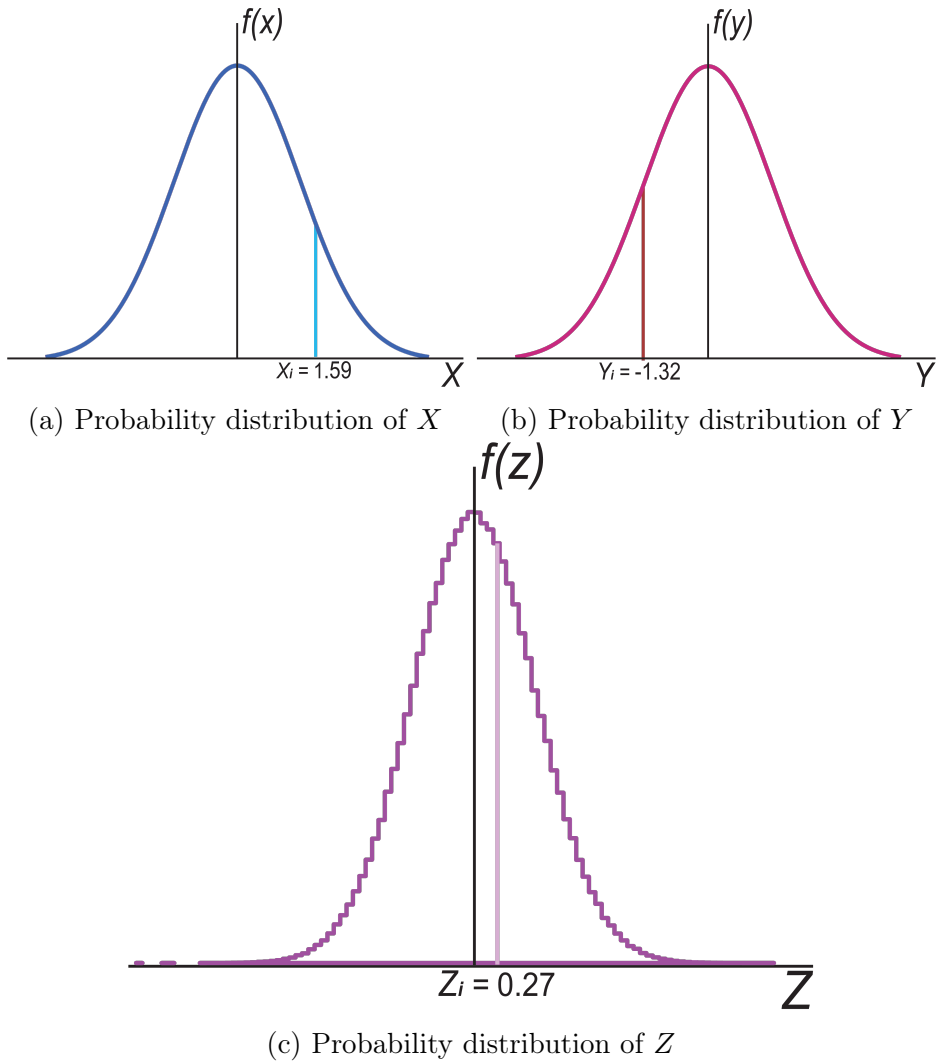


Figure 2-1: Probability distributions for (a)  $X$ , (b)  $Y$ , and the (c) Monte Carlo results for  $Z$  in our Monte Carlo toy model. The results of trial  $i$  are highlighted.

While the normal distribution seems to be a natural choice for a probability distribution, it has some drawbacks. The normal distribution is not bounded; there always exists some probability of choosing an arbitrarily negative value for some parameter. This can be a problem, since for most parameters the value should always be greater than or equal to zero. For example, manufacturers are not being paid to install a sputterer. Negative values are clearly unrealistic and can make the model's results unreliable.

## Log-normal Distribution

One simple method of circumventing this issue is through the log-normal distribution. It is defined such that, for a standard normal random variable  $Z$ , the log-normally distributed random variable  $X$  with median value  $\mu$  and scale determined by  $\sigma$  is defined as

$$X = e^{\mu + \sigma Z}$$

This has the nice property of yielding strictly positive values, unlike the normal distribution. However, the log-normal distribution is only parameterized by  $\mu$  and  $\sigma$ , which means that the high and low estimates for a given parameter are forced to be related to each other. This may not be a significant issue for some parameters, but if the modeller would like more flexibility in their probability distribution, other choices should be pursued. Like the normal distribution, the nominal estimate is set as the median of the distribution, the low estimate is defined to be the 10th percentile, and the high estimate is set as the 90th percentile.

## Triangular distribution

There are two common distribution types in finance which allow the modeller to flexibly choose low, nominal, and high estimates for their parameters. One of these is the triangular distribution, which is defined by a lower bound  $a$ , mode  $c$ , and upper bound  $b$ . This is useful as a "lack of knowledge" distribution, where the modeller has little information on the actual probability distribution but has an educated guess on a most likely value as well as boundary values the modeller knows the parameter cannot surpass[13]. The triangular distribution is defined as

$$f(x) = \begin{cases} 0 & \text{for } x < a \\ \frac{2(x-a)}{(b-a)(c-a)} & \text{for } a \leq x \leq b \\ \frac{2}{(b-a)} & \text{for } x = c \\ \frac{2(b-x)}{(b-a)(b-c)} & \text{for } a \leq x \leq b \\ 0 & \text{for } x > b \end{cases}$$

For triangular distributions in our model, we define the low estimate as  $a$ , the nominal estimate as  $c$  and the high estimate as  $b$ .

### Beta-PERT distribution

Similar to the triangular distribution, the beta-PERT distribution is defined by a lower bound  $a$ , mode  $c$  and upper bound  $b$ . The biggest difference between the triangular and beta-PERT distributions is that the mode and extremes are weighted differently. For the triangular distribution, the end-points are weighted more strongly. For example, the mean for the triangular distribution is defined as  $\mu = \frac{a+b+c}{3}$ , which weights the endpoints and mode equally. This is often unfavorable, since estimation of extremes is often poor compared to estimation of the mode. The beta-PERT distribution is also smoother. This means values around but not equal to the mode are weighted more highly and values near the endpoints are weighted less highly, which is often more realistic[13].

In addition to the bounds and mode, the beta-PERT distribution is also parameterized by a scale factor  $\lambda$  which determines how strongly the mode is favored over the endpoints. The probability distribution, shown in Figure 2-2 is calculated as follows:

$$\mu = \frac{a + b + \lambda c}{\lambda + 2}$$

$$v = \frac{(\mu - a)(2c - a - b)}{(b - a)(c - \mu)}$$

$$w = \frac{v(b - \mu)}{\mu - a}$$

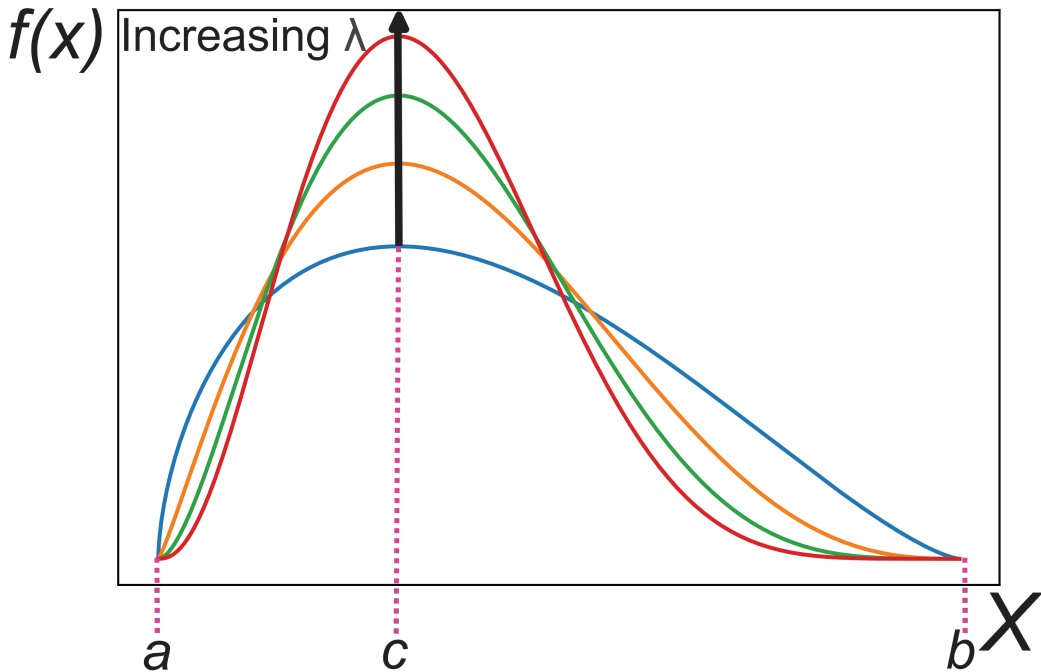


Figure 2-2: Visualization of beta-PERT distribution. The distribution goes to zero at the endpoints, and increasing lambda makes the peak larger and narrower.

$$f(x) = \frac{(x-a)^{v-1}(b-x)^{w-1}}{B(v,w)(b-a)^{v+w-1}}$$

where  $B(v, w)$  represents the beta function. Like the triangular distribution, in our model we define the low estimate as  $a$ , the nominal estimate as  $c$ , and the high estimate as  $b$ .

## 2.3 Defining a Manufacturing Sequence

In this section, we will discuss the module stacks and manufacturing sequences we would like to model. We assume a 100 MWp/yr factory located in the United States to define our factory assumptions, and reference the standard literature as well as industry sources for data on parameter values.

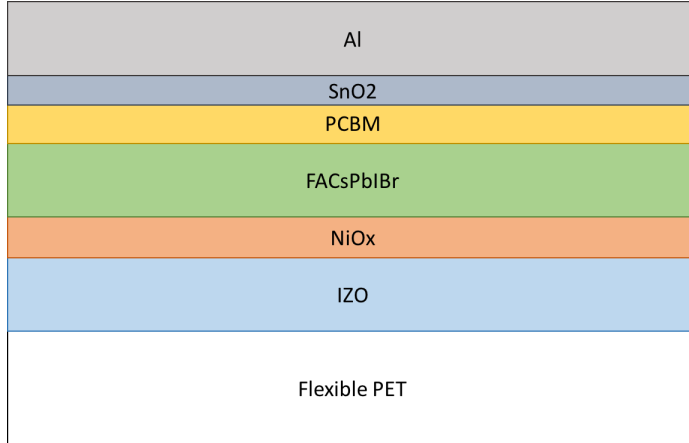


Figure 2-3: Perovskite solar cell structure

### 2.3.1 Single Junction Perovskite Reference Module and Manufacturing Sequence

Here we consider the design of a standard single junction perovskite module. We elect to use indium zinc oxide (IZO) coated on a flexible polyethylene terephthalate (PET) substrate. Not only does this flexibility allow for new applications with lightweight flexible solar cells, it could potentially cheapen the manufacturing process with R2R manufacturing. The active material we use is a mixed iodide-bromide formamidinium-cesium-lead perovskite ( $\text{FACsPb}(\text{IBr})_3$ ), which has been shown in Leijtens et al. to have improved stability over traditional  $\text{MAPbI}_3$  perovskites[15].

Nickel oxide (NiOx) is used as the hole-transporting layer. We opt for PCBM as the electron transport layer. For the rear metal we use a thin layer of aluminum. The full stackup is shown in Figure 2-3.

For our manufacturing sequence, we assume a continuous R2R line in a 100 MW factory. The IZO and Al electrodes are sputtered, followed by laser scribing. The charge transport layers are similarly sputtered. We choose to slot die coat the perovskite. A flow diagram of the entire manufacturing process is shown in Figure 2-4. A full list of cost input parameters for our manufacturing sequence is included in Appendix A.

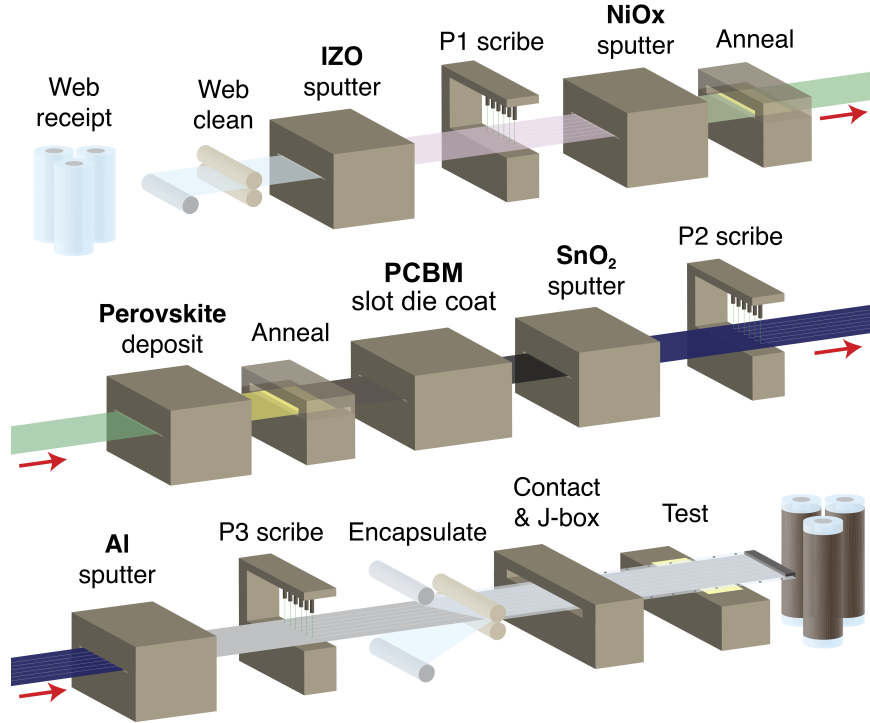


Figure 2-4: Diagram of roll-to-roll manufacturing sequence for perovskite solar modules

## 2.4 Cost Model Results

We modeled the cost for the given sequence and plotted the Monte Carlo cost distribution. The model was performed with 100000 trials, which should reduce any probability error to negligible amounts. The cost is presented in  $\$/m^2$  as manufacturing cost in Figure 2-5, while cost in  $\$/W$  is plotted in Figure 2-6. The  $\$/W$  figure gives an idea for base PV cost, and is dependent on the module efficiency. We assume for this analysis a conservative efficiency of 15%. The conversion between cost  $C$  in  $\$/m^2$  and  $\$/W$  can be calculated as

$$C_W = \frac{C_{m^2}}{PCE \times P_0}$$

where  $P_0$  is the irradiance power density under standard test conditions ( $1000 \text{ W/m}^2$ ).

The median, 10th percentile, and 90th percentile costs in both  $\$/m^2$  and  $\$/W$  are presented in Table 2.4.

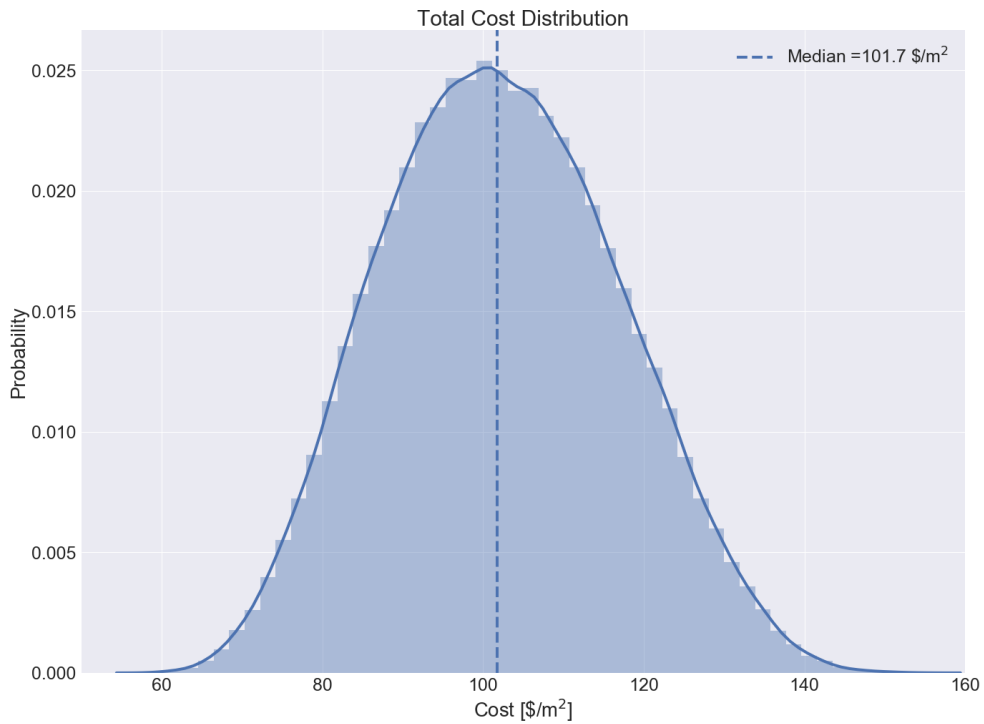


Figure 2-5: Manufacturing cost distribution in \$/m<sup>2</sup>

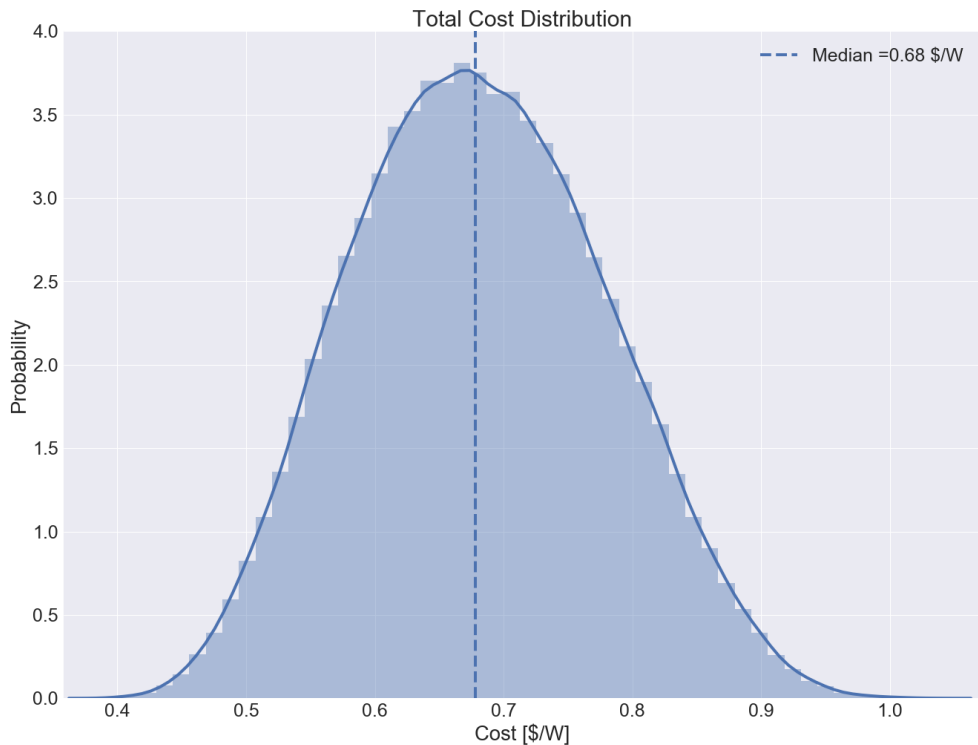


Figure 2-6: Manufacturing cost distribution in \$/W

<i>Units</i>	<i>Median</i>	<i>10th Percentile</i>	<i>90th Percentile</i>
\$/m <sup>2</sup>	101.7	83.1	121.8
\$/W	0.68	0.55	0.81

Table 2.4: Cost distribution results, assuming a 15% module efficiency

We see that, compared to the \$0.40/W manufacturing cost of silicon PV, this perovskite PV process can be as high as twice as expensive, at up to potentially \$0.81/W. To see what drives the price, we can plot the 5 largest cost components. In doing so, we can determine which cost components to focus research efforts on to reduce the price. The 5 largest cost components for our manufacturing sequence is plotted, in \$/m<sup>2</sup>, in Figure 2-7.

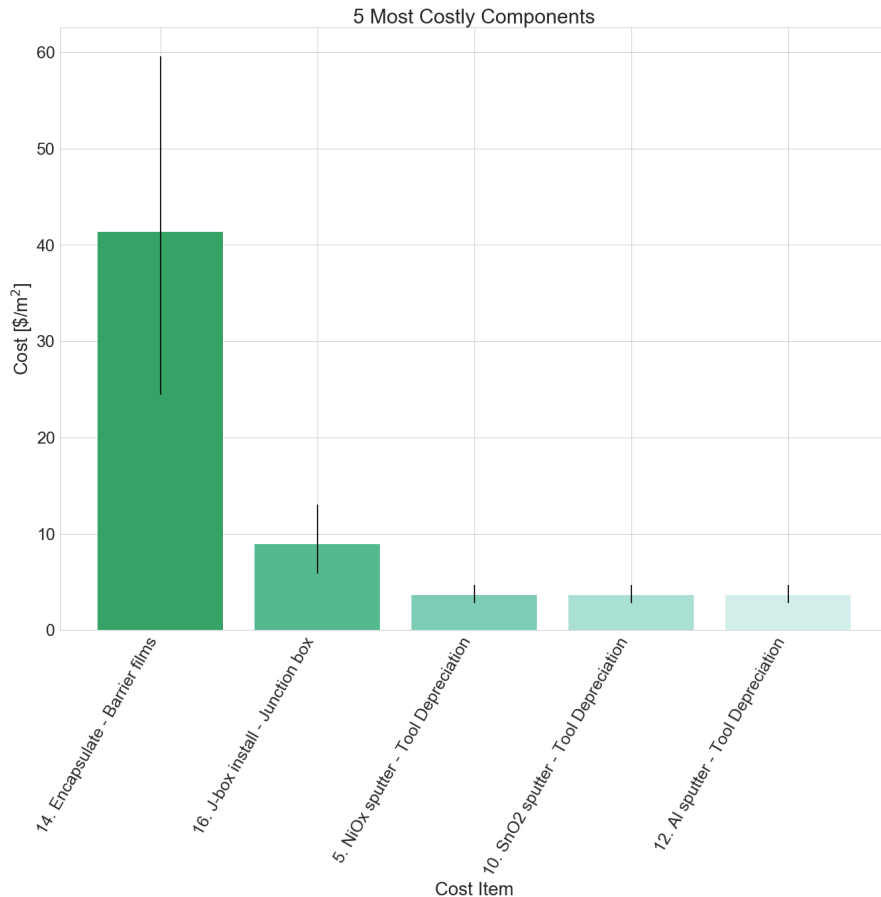


Figure 2-7: The 5 most costly components of the given manufacturing sequence in \$/m<sup>2</sup>. Error bars indicate the 10th and 90th percentile estimates for each component's cost.

We see that the barrier film dominates the cost. Rather intuitively, the sputtering tools are very costly as well. The junction box, as a discrete component, also contributes significantly to the cost.

It is also useful to breakdown the cost by process so that we may understand how to optimize each step. The costs for each process is visualized in Figure 2-8. As expected from the cost component breakdown, the encapsulation step is by far the most expensive, dominated by materials cost due to the expensive barrier layer. Additionally, the deposition steps (sputtering and slot die coating) are noticeably more costly than the others. An interesting and encouraging result to point out is the cheap cost of the perovskite material itself, which is one of its main draws from a cost perspective. The materials component of the FaCsPbIBr slot die coat process is essentially negligible, at only \$0.50/m<sup>2</sup>.

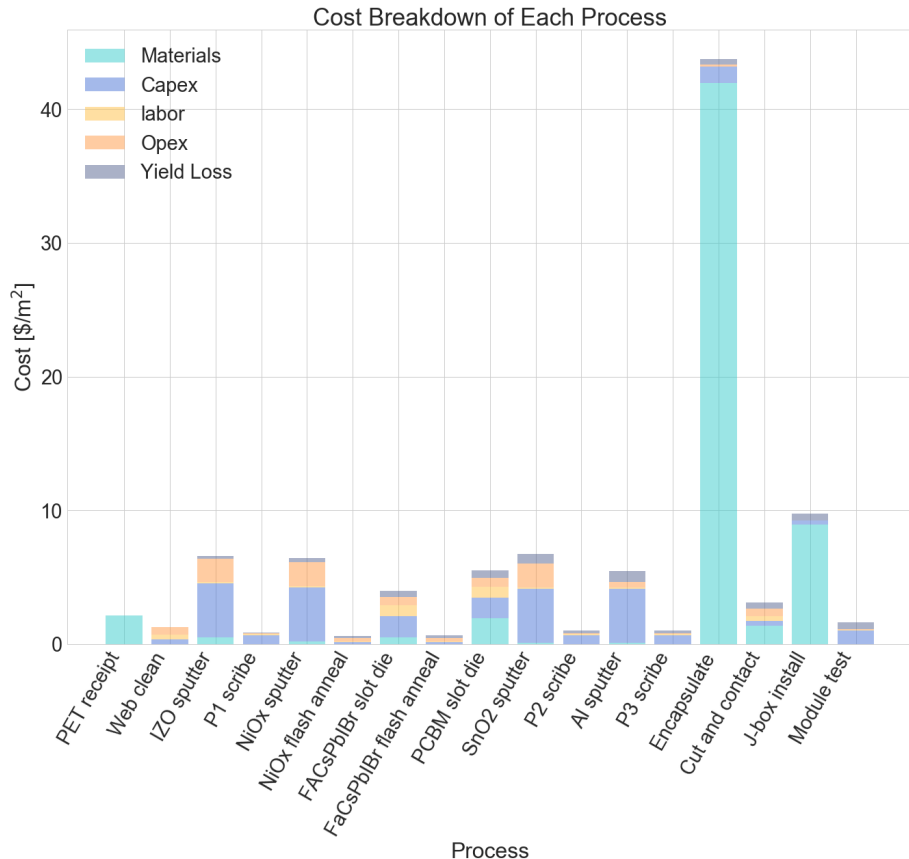


Figure 2-8: Manufacturing sequence cost breakdown by process in \$/m<sup>2</sup>, broken down by materials cost, capex, labor, opex and cost associated with yield loss.

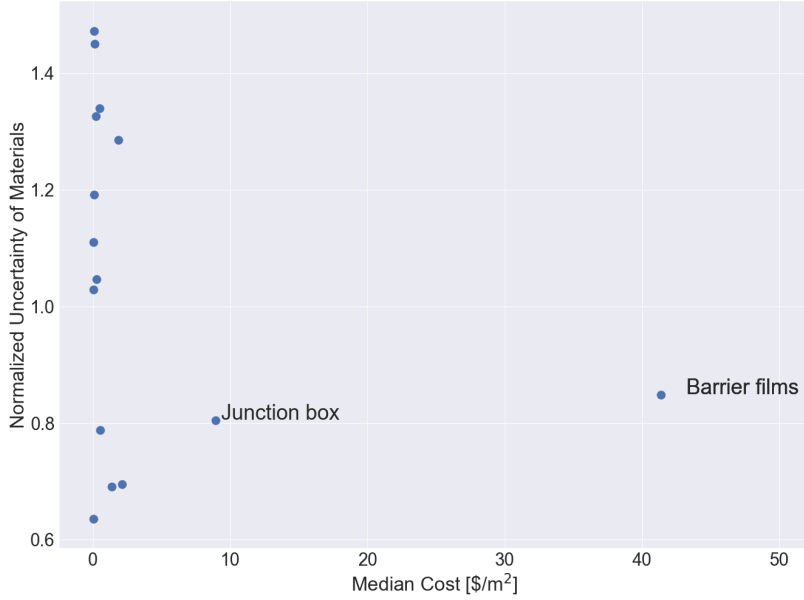


Figure 2-9: Normalized uncertainty of materials costs

In order to tighten our bounds on the actual cost of the sequence, we must reduce uncertainty. To do so, we must see which cost components contribute the most to our uncertainty. A useful visualization of this is a plot of the normalized uncertainty over median price, where normalized uncertainty is defined by the difference between the 90th percentile cost estimate and the 10th percentile cost estimate, all over the median cost estimate. The points with high median cost as well as high normalized uncertainty are worth examining in that, a lower cost might be found for these components, or a tighter bound can be created which would reduce the total uncertainty. The normalized uncertainty plots are shown in Figures 2-9 and 2-10. From the plots, it appears that both the barrier film and junction box have large uncertainty relative to their median cost, and are worth investigating to refine the bounds. Similarly, the sputtering tools are large contributors to the uncertainty.

## 2.5 Discussion

Our cost model predicts a promising nominal estimate of \$0.68/W. A staggering 40% of this comes from the barrier films alone, as a high quality encapsulant is likely needed to prevent perovskite degradation. While a large uncertainty is reported for

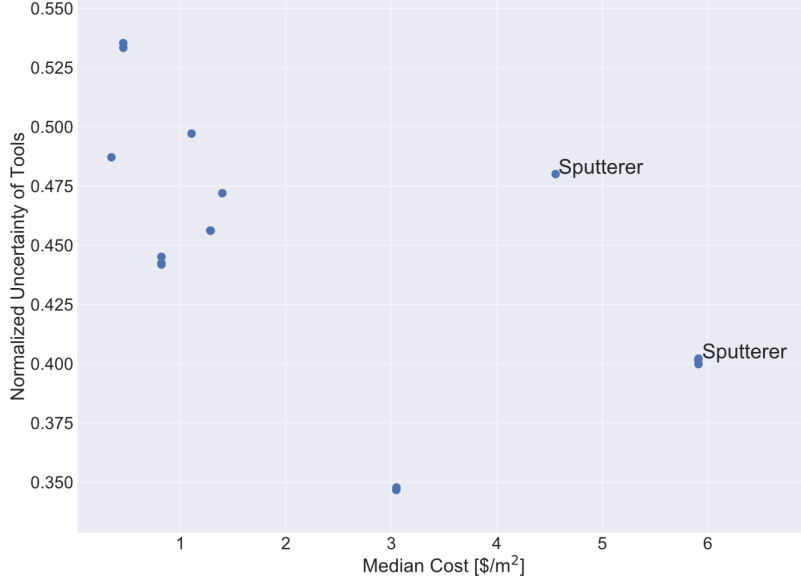


Figure 2-10: Normalized uncertainty of tools costs

the barrier film, this is mostly due to the fact that film cost scales directly with quality - depending on the application's lifetime requirement, a cheaper or more expensive film may be required. Even so, much work must be done to optimize this portion of the cost for flexible perovskite PV to become more cost competitive.

The sputterers are also large cost contributors in the form of capex. If we were to increase the throughput of the R2R line, the tool depreciation cost, which is inversely proportional to throughput, would decrease. The depreciation cost as a function of throughput for a \$6.5M sputterer in a factory operating 3690 hours a year is plotted in Figure 2-11. We see that an increase in throughput from the current nominal estimate of 67 m<sup>2</sup>/hr to 100 m<sup>2</sup>/hr would result in a decrease of \$5/m<sup>2</sup> across the R2R line, which is a 5% decrease in final cost. While not a huge decrease, shaving costs wherever possible could be a worthwhile endeavor.

Another method to achieving cheaper \$/W cost is through improving efficiency. If we produce modules at a more optimistic efficiency of 20%, we find the median per watt cost dropping from \$0.68/W to \$0.51/W, which is a fairly dramatic decrease and brings perovskite PV closer to the silicon PV manufacturing price.

Since we performed a Monte Carlo analysis and accounted for as much uncertainty as possible, it is very likely the true cost falls within the estimated cost distribution.

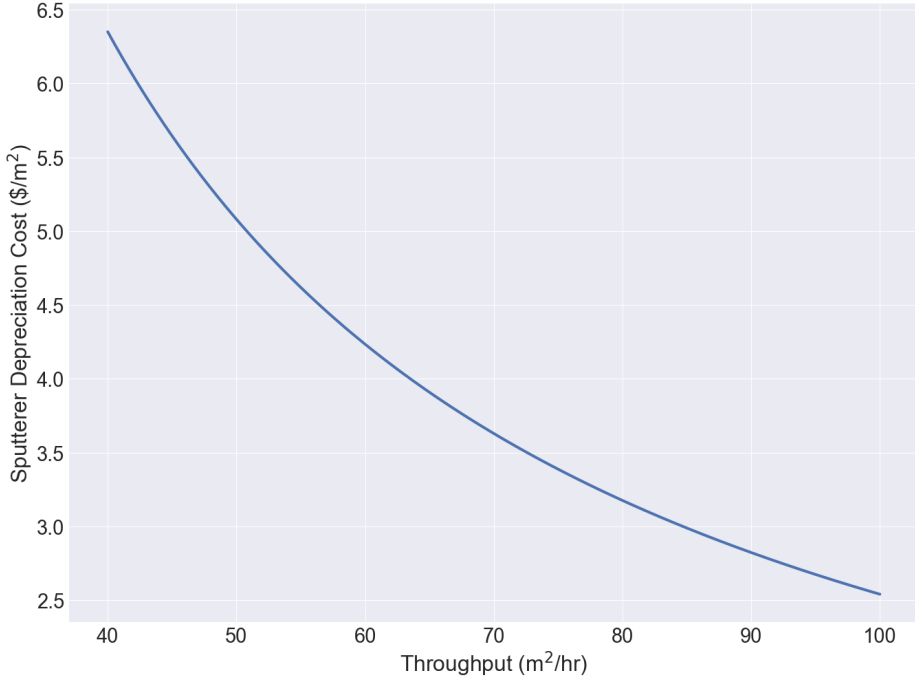


Figure 2-11: Sputterer depreciation cost as a function. This assumes a \$6.5M sputterer in a factory operating 3690 hours a year with a depreciation period of 7 years.

However, we perform some simplified assumptions in our cost model; for example, we assume that Monte Carlo results for all parameters in a trial are independent, when in reality they would not be. For instance, the throughput across every tool should be the same for an R2R line, but is calculated individually for each tool in the model for a single trial. This discrepancy is assumed to have little impact on the final result, as any such fluctuations would average out over many Monte Carlo trials.

In real-world applications, we are mostly concerned with the cost of PV systems on a per watt basis. This number includes not only the module manufacturing cost, but also costs associated with installation and profit. In the next chapter, we apply the results from our cost model, combined with installation cost and profit assumptions, to the case of installing perovskite PV on telecommunications towers.

## **2.6 Chapter Acknowledgements**

I would like to thank Joel Jean, who provided input on the cost model, provided many of the numbers for the cost inputs, and defined the manufacturing sequence. Sarah Sofia provided many of the numbers for tool costs.



# Chapter 3

## Economics of Vertically Deployed Photovoltaics on Telecommunications Towers

In addition to being cheap enough to enter the market, lightweight flexible PV needs to have applications not currently fulfilled. For instance, being lightweight and flexible means perovskite PV can be easily transported to remote areas, or mounted on less reinforced structures. This seems especially relevant for developing countries, where PV must be driven long distances on flatbed trucks to remote villages. In this chapter, we will investigate a possible market application: powering telecommunications towers.

### 3.1 Telecommunications Towers: A Background

As global demand for connectivity grows, the necessity of telecommunications towers continually increases. This translates to building more towers worldwide, with increasing demand for power as more users access each tower. While the United States enjoys a well connected and reliable grid system, the same cannot be said in other countries.

As an example, American Tower Corporation (ATC) owns tens of thousands of

towers in India, Ghana, Uganda and Nigeria. For many of the towers, the grid can be so unreliable that it powers the tower for only a few hours a day. A large percentage of the towers are completely off-grid, running for the most part on diesel generators and batteries.

On the short term, using diesel works decently well, and sufficiently covers power demand for the towers. However, there are significant drawbacks to using diesel. For instance, diesel in India currently hovers around \$1/L[3], which is quite expensive and can accumulate in operating cost over a long period of time. Even worse, as time goes on, diesel cost is trending up. Additionally, diesel generators (DG) are very inefficient at around 15% power efficiency, which means most of the diesel energy is wasted.

In addition to diesel cost, there are some drawbacks related to supply chain. Transporting diesel to distant rural tower sites represents a drain on both time and financial resources, which adds even more opex. An interesting but problematic challenge that is being continually faced at telecommunications sites in India is the theft of diesel, which adds a risk factor and increasing cost in powering these towers.

Finally, and arguably more importantly, diesel generators pose environmental risks due to carbon emissions. One liter of diesel translates to 2.68 kg of carbon dioxide[4]. As a back of the envelope calculation, if a tower consumes 2.5 L of diesel per hour and runs on diesel for 12 hours a day, then a total of 30 tons of CO<sub>2</sub> is produced in only one year. In comparison, the average UK household CO<sub>2</sub> emission in 2012 was around 20 tons per year [17]. This is a fairly significant amount, and with thousands of towers lasting tens of years, it is safe to say that DG-powered towers contribute to the carbon emission problem.

One possible way to help curb these issues is the installation of renewable energy to power the towers. Adding solar panels as a source of power could supplement (and potentially replace) the use of diesel to power the tower. However, for towers with larger power demands, a larger area of solar modules is required. This may not be feasible as many towers have only a small area of land available, as small as 400 ft<sup>2</sup>. On the other hand, for a standard 150 foot tall tower, only the top 50 feet are utilized. The rest of the 100 feet represent available and unused vertical real estate,

which would be suitable for installing solar panels. Traditional silicon panels are very heavy, however, which makes it typically unfeasible to install significant amounts of c-Si PV along the tower. A solution to this issue is the use of lightweight perovskite solar cells, which would not represent a significant weight to the tower and can be installed vertically.

Though the weight problem would be solved, there are other issues that must be considered. On the structural side, a large flat area installed along the side of the tower could potentially dramatically impact the wind load of the tower. It becomes important to consider the effects of this increased wind load and determine if the tower's structural stability would be compromised.

Another important factor is the economic impact of the solar installation. If installing PV becomes a financial burden, there is little incentive to adding solar to power the towers. Thus, we would like to use the results from our cost model to determine whether it is economically feasible to install PV to the towers as a diesel/solar hybrid power source. To this end, we use the microgrid simulation software HOMER to calculate the costs of diesel/solar versus using diesel alone.

## 3.2 Wind Loading on Telecommunications Towers with PV

We now discuss the effect of vertically mounted PV on tower wind loading. We will first discuss some methods of calculating wind load to develop an intuition, followed by finite element analysis results. Modeling is performed with a typical 45 m, 4-leg lattice tower. A 40 m/s wind speed is assumed. We will follow the TIA-222-G standard, which tower wind loads are designed to follow[1].

In order to get accurate results, we can simulate the effect of adding panels to the tower. We thus apply finite element analysis on the tower and add different size panels to determine the limit at which the tower deforms according to the TIA-222-G standard, or where the max stress on the tower exceeds the allowable stress of the

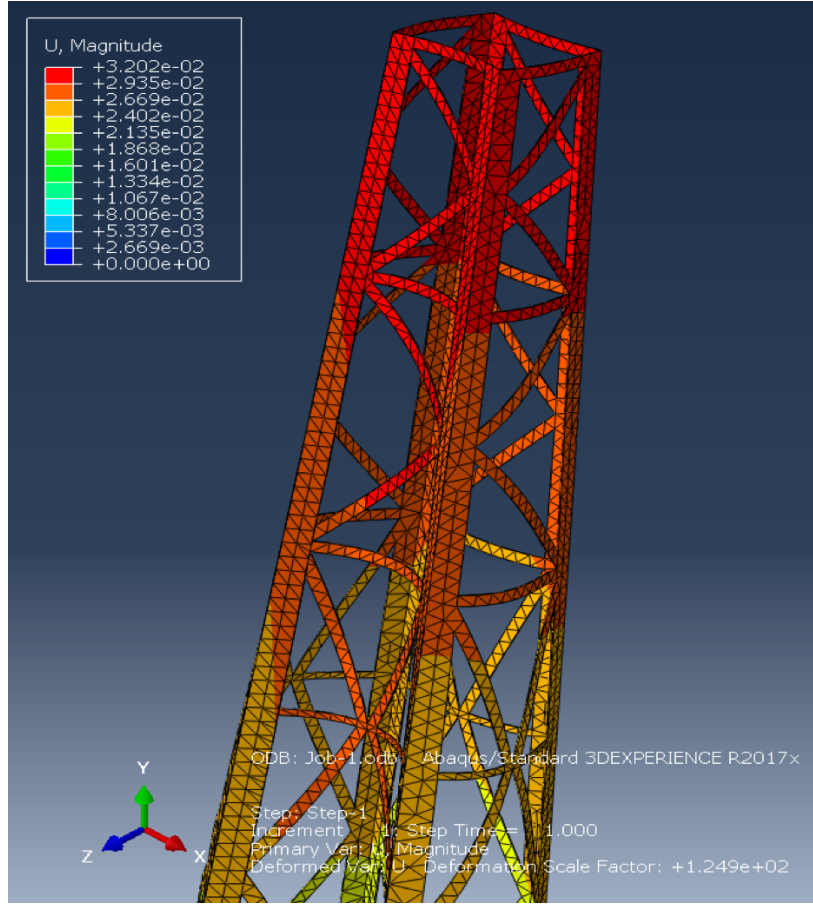


Figure 3-1: Deflection of tower under maximum wind load with no PV

steel. In this case, the steel has a max allowable stress of 470 MPa, and with a safety factor of 2 we do not want any member of the tower to have a stress exceeding 235 MPa.

Assuming a typical 45 m tower, it is found that in the base case, a tower under 40 m/s wind experiences a 35.38 kN force. If we were to apply PV to only existing members (i.e. add PV without increase wind load), we find that the tower deflects merely 32 mm, which translates to  $0.02^\circ$ . This is shown in Figure 3-1. The maximum stress in this case comes out to 37 MPa, well below our limit.

We also simulated cases for rectangular panels covering an entire side with width 888 mm and 4888 mm (the min and max width along the tower), as well as a trapezoidal panel completely covering a side. The wind load is applied perpendicularly to the panels. The results are summarized in Table 3.1.

Case	Additional Panel Area ( $m^2$ )	Deflection (degrees)	Max Stress (MPa)
No panels/panels on existing members	0	0.0229	37
888 mm wide panel	39.96	0.0758	107
Trapezoidal panel	119.6	0.1816	247
4888 mm wide panel	199.96	0.2777	388

Table 3.1: Wind force on different panel geometries

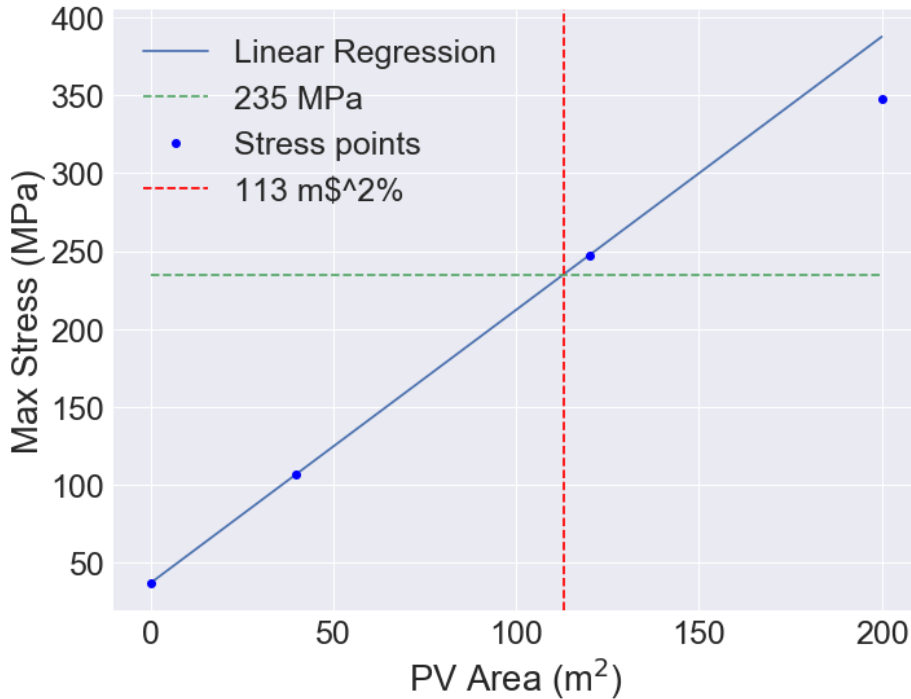


Figure 3-2: Linear regression to find the maximum allowed PV area

We notice from these results that the max stress is the limiting factor on our panel size, and actually scales very linearly with panel area. We can form a linear regression, visualized in Figure 3-2, to find the panel area at which the max stress is 235 MPa. We find a maximum area of 113  $m^2$  which, for a 15% efficient cell, comes out to a maximum 16.95 kWp of installed PV. We thus conclude that the tower is not the limiting factor on wind load - instead, we must be able to design the PV to withstand the wind loads. In simulating the towers with 300  $\mu m$  thick PET panels, the PV fails long before the tower does. Thus, either sturdier panels or a system to retract the panels during high wind are desired.

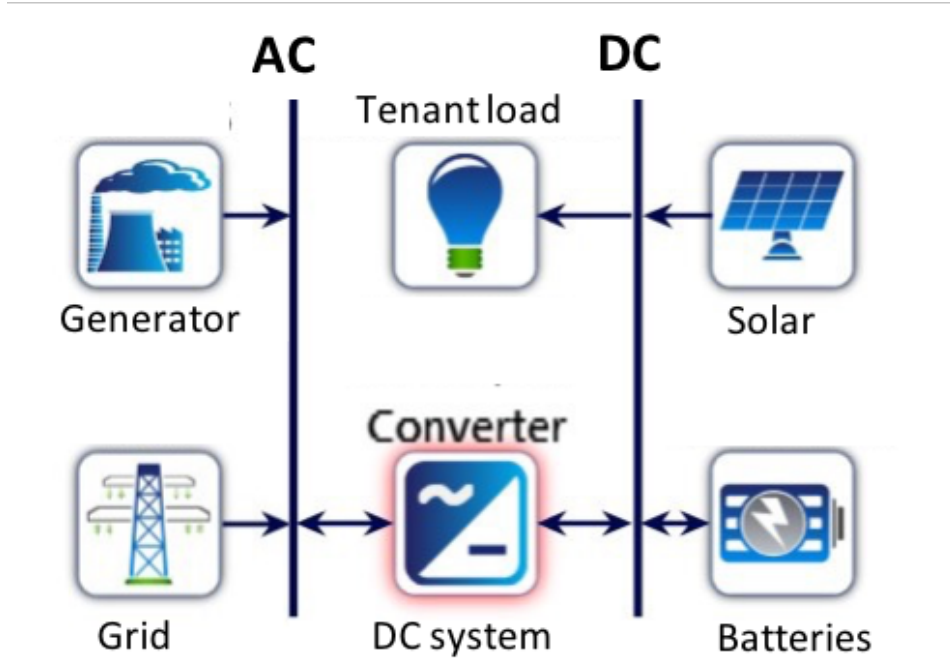


Figure 3-3: Schematic of HOMER inputs

### 3.3 HOMER Microgrid Simulation

In order to perform a thorough financial analysis, we use a software called HOMER. Developed by NREL, HOMER is a microgrid optimization and design software that optimizes power systems based on net present cost (NPC), which is the total cost of the system over its lifetime. By providing information on the location (and thus solar insolation profile), PV system, diesel generator, batteries, grid, converter and load, HOMER will optimize for the configuration with the lowest NPC that still satisfies the load[2].

We can also include sensitivity analysis on any input variable, so that we may see the impact that changing the value of that variable will have on the optimal system.

#### 3.3.1 Defining Our HOMER Model

For our analysis, we would like to see how financially feasible deploying PV in countries such as Nigeria, Uganda, Ghana and India is. In particular, Nigeria and India present

interesting cases, as Nigeria has a particularly low diesel cost at \$0.55/L and India has variable grid reliability but a more standard diesel cost of \$1.02/L [3]. We will thus perform simulations in Maiduguri, Nigeria and Rajasthan, India, which both have high solar potential.

We begin the HOMER model by defining the system economics. Here, the variables of interest are model period, inflation, WACC, and real discount. The first variable of interest is the model period. This defines the time over which the financial analysis is run. We also include inflation, which is the expected inflation rate over the course of the system lifetime. Weighted average cost of capital (WACC) represents the cost of the company's debt and equity. Real discount is the rate which the company can borrow money.

For the diesel generator, the variables of interest are the initial/replacement cost, lifetime, O&M cost, fuel price, and fuel consumption. The initial/replacement cost is the capital cost of installing or replacing the generator. Lifetime is the number of hours that the generator can run before needing to be replaced. O&M cost is the cost of operating/maintaining the generator per year. Fuel price is the price of diesel in the area of interest. Fuel consumption is the amount of fuel required to run at different loads; generally, higher power loads are more efficient. This fact can lead to somewhat unintuitive results, which we discuss later. The main variable of interest here is the diesel cost, as its value varies significantly across different countries as well as over time. Thus we are interested in performing sensitivity analysis on diesel cost.

For the grid, the three input variables we set are the cost of energy in \$/kWh, grid reliability in hours per day, and variance in reliability. Grid reliability is an especially interesting variable for us, as India in particular has very different grid reliabilities across the country. We thus want to be able to predict how this variation will affect tower economics and apply sensitivity analysis to this variable.

The batteries also play an important role in the system, storing and leftover energy produced by the DG or PV. We define the battery capacity in Ah, the battery cost, lifetime throughput in kWh, and its lifetime in years. The variable of interest here is the battery cost, as lithium-ion batteries are expected to halve in price in the next

ten years. Thus, we apply sensitivity analysis on the battery cost.

Of course, we need to define the PV system. This takes in as variables the maximum PV size, PV cost, lifetime, and derate factor. The maximum PV size is set by the wind loading analysis, which gave a maximum size of  $100 \text{ m}^2$ . Assuming a 15% module efficiency, this translates to a max PV size of 15 kWp. PV cost is the cost in \$/W. If we assume a balance-of-system cost of \$0.50/W and an installation labor cost of \$0.24/W, and include a profit margin of 17%, we get a system cost between \$1.51/W and \$1.82/W from our cost model. To be conservative, we estimate the final system cost to fall between \$1.5/W - \$2/W in this analysis. Since PV price is particularly important, we apply sensitivity to PV cost in all simulations. For perovskite PV, as a young technology known for being unstable, it is important to see how changing the lifetime affects the system economics, so we also simulate lifetime as a sensitivity variable. Finally, derate is a factor that represents "real world efficiency" - that is, how much do real world considerations such as dust, shading and wiring loss affect PV output. We are also interested in this as a sensitivity variable, as it encapsulates degradation in PV efficiency over time which is a potential problem with perovskite PV. We also set the tilt angle to  $85^\circ$  (the approximate tilt of a tower side) and the azimuth to  $0^\circ$  such that the panel faces south.

Finally, we define a DC/AC converter and tenant load. The converter has an associated cost, lifetime and power capability, while the load is simply the power demand of the tower. We assume an average load of 5 kW for the tower.

Some approximate values for key inputs, informed by discussion with ATC, are given in Table 3.2. Battery cost is given as \$ per 48V, 80 Ah battery.

### 3.4 Simulating Tower Microgrids in Nigeria

One of the primary countries of interest to install PV is Nigeria. This is due to its low diesel price, which disincentivizes improving the grid, as well as high solar insolation. However, this low diesel price may also make vertical PV installation less attractive. We thus run HOMER simulations applying sensitivity on diesel price,

<i>Base Input Assumptions</i>	
Diesel cost in Nigeria	\$0.55/L[3]
Diesel cost in India	\$1.02/L[3]
Battery cost	\$2000
PV derate	80%
PV lifetime	10 years
Grid reliability in Nigeria	5 hrs/day
Grid reliability in India	12 hrs/day

Table 3.2: Base assumptions for key Nigeria microgrid simulation inputs

battery cost, PV lifetime, PV derate, and grid reliability all over PV cost sensitivity ranging from \$1/W - \$3/W. These studies are performed with and without grid. The full results are presented online on at <https://github.com/jtxiao/Vertical-PV-on-Tower-HOMER-Results>.

### 3.4.1 HOMER Results

In the case of Nigeria, it is found that the results are not significantly different between the cases of with grid and without grid. Additionally, the sensitivity variable that has the most impact on optimal system configuration is diesel price. Thus, we look at the impact of diesel price with no grid by plotting heat maps of optimal PV size, NPC, renewable fraction, and fuel diesel usage reduction plotted in Figures 3-4 - 3-7. We force a minimum PV size of 1 kW<sub>p</sub>, even if it is unfavorable financially, such that we can determine the impact it will have on NPC, renewable fraction and diesel reduction. For NPC, we plot the percent change in NPC by installing PV compared to the case without PV. Renewable fraction is defined as the fraction of the energy delivered to the load that comes from renewable sources.

It is worth noting that the numbers for renewable fraction do not include energy delivered by the batteries, which store a large amount of the energy produced by PV. Thus, the number underestimates the total amount of energy from the PV system.

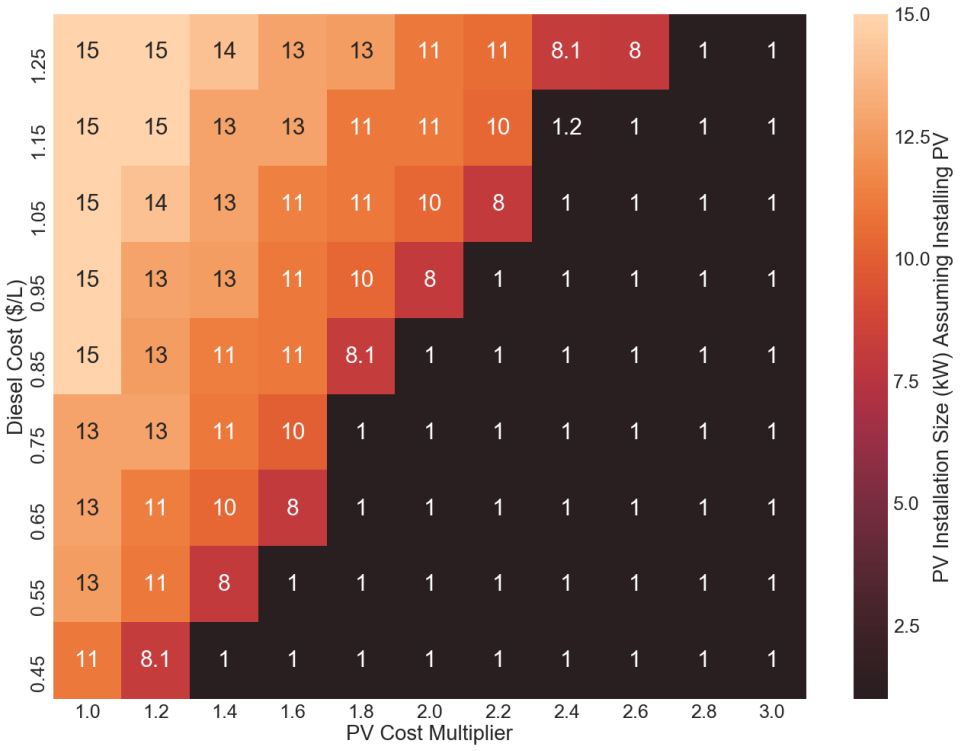


Figure 3-4: Heat map of optimal PV installation size (1 kWp minimum) with varying PV cost and diesel cost in Maiduguri, Nigeria.

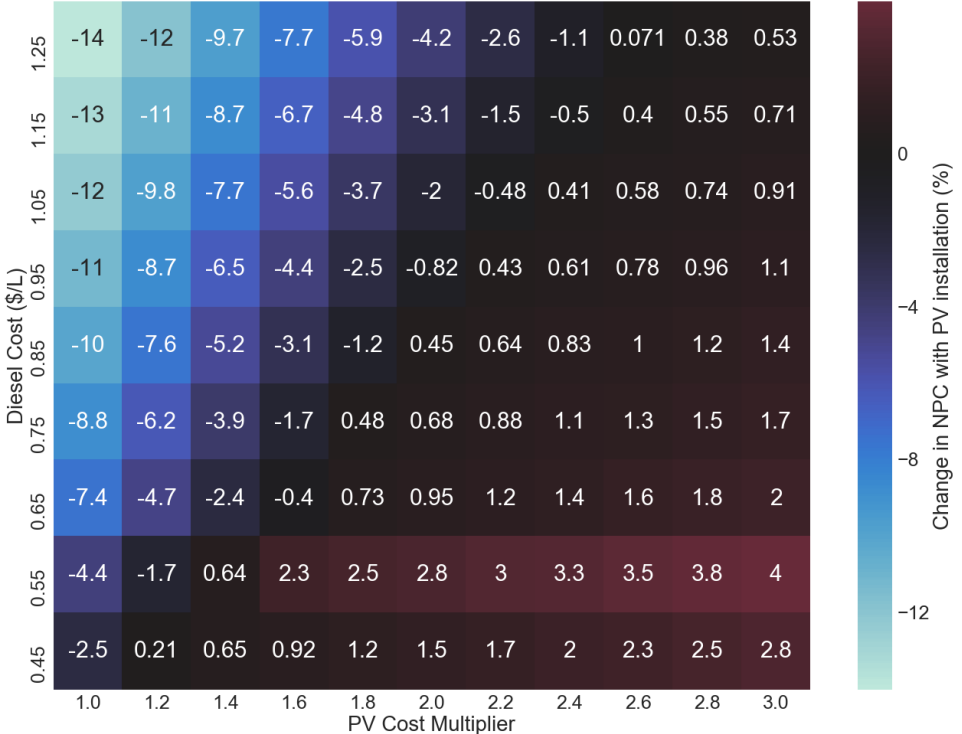


Figure 3-5: Heat map of change in net present cost given the PV installation in Figure 3-4 with varying PV cost and diesel cost in Maiduguri, Nigeria.

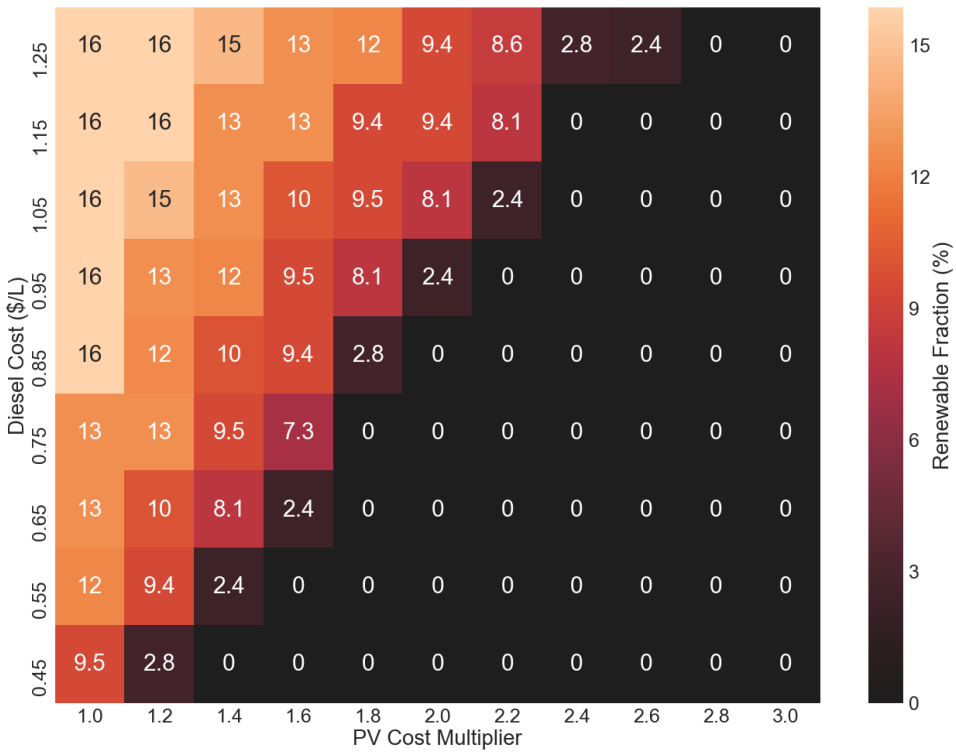


Figure 3-6: Heat map of renewable fraction given the PV installation in Figure 3-4 with varying PV cost and diesel cost in Maiduguri, Nigeria.

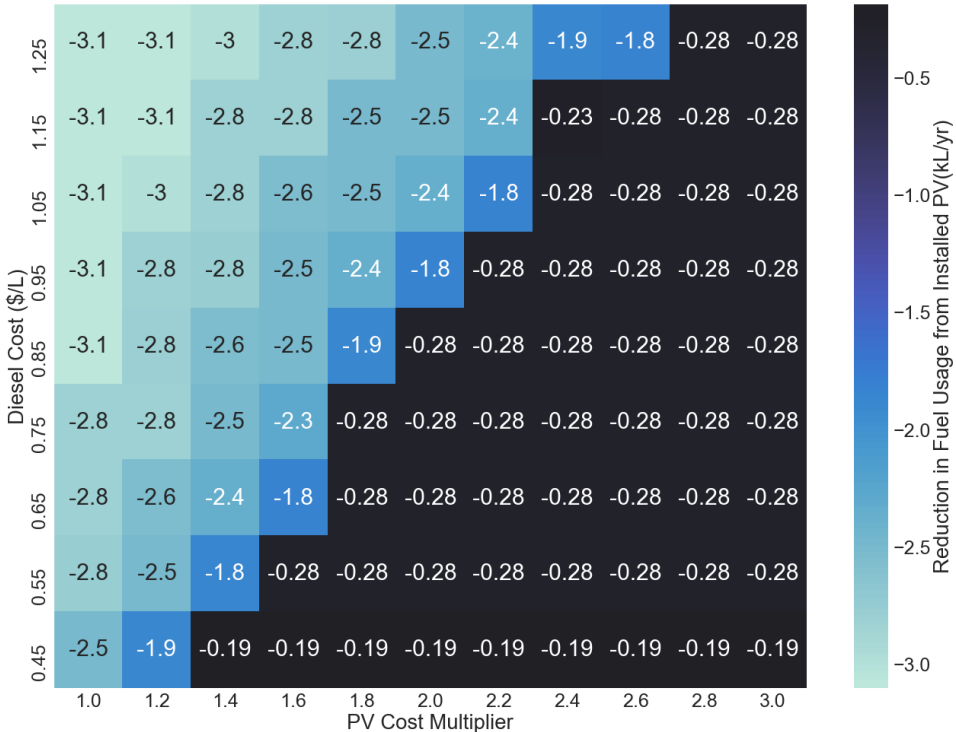


Figure 3-7: Heat map of change in diesel usage reduction given the PV installation in Figure 3-4 with varying PV cost and diesel cost in Maiduguri, Nigeria.

### 3.4.2 Is Vertical PV Financially Viable in Nigeria?

Given that the diesel price in Nigeria currently sits at \$0.55/L, and that the projected price of perovskite PV is between \$1.5/W - \$2/W, we see from the HOMER results that the optimal system from these inputs has no PV installed. If we force a 1 kW<sub>p</sub> system installation, we see a somewhat large increase in NPC (between 2.3% and 2.8%). This shows that, from a cost perspective, it does not make sense to install vertical PV on the towers.

However, the main draw of solar energy need not be purely a financial one. Nonetheless, we see that, even if we install some PV, we just do not see a significant reduction in fuel usage at only 280 L/yr. Virtually none of the energy delivered to the load comes from a renewable source. Installing PV does not seem significantly greener, in this case.

That being said, all hope is not lost. Diesel prices globally are on the rise. In Nigeria alone, diesel prices have skyrocketed in the last 15 years, going from \$0.19/L to \$0.55/L. It is not unreasonable to expect a doubling in diesel price in the next 10 years, bringing the cost to approximately \$1/L. Referencing Figure 3-4, we see that this price encourages the installation of a large amount of PV. Even better, solar prices are expected to decrease significantly in this time, making PV even more attractive.

This fact is actually very encouraging, as the global average diesel price sits around \$1/L. In fact, India, one of our main target countries, has a diesel price of \$1.02/L. Thus, we would like to now focus our analysis on India.

## 3.5 Simulating Tower Microgrids in India

While India rapidly modernizes, the need for electrification rises. As such, oil is India's number one import[26]. One challenge being faced is that grid energy in India can be unreliable - in fact, 240 million people currently do not have access to electricity[23]. One of the main energy goals set by the government is "24x7 electricity for all", including 100 GW of solar, by 2022[12].

In parallel with the need for energy is the need for access to communication. Modernization in India has introduced many to cell phones, and with the rise of cell phones comes the need for more telecommunications infrastructure. Companies like ATC own thousands of cell towers and are continuously building more. As each tower is built, the question arises on how to power the tower. With low or non-existent grid reliability, powering towers with diesel seems like a straightforward and relatively cheap option. However, diesel is often stolen and poses environmental risk.

Because of government support and its tropical location, India makes a prime target for PV installation. This makes a solar/diesel hybrid solution an attractive candidate for powering communications towers. We now analyze the economics of powering telecommunications towers with vertical PV in order to determine whether it makes financial sense.

### 3.5.1 HOMER Results

In the case of India, we run the same analysis as in Nigeria, but focus on grid reliability as that is the main variable of interest in India. Again, the full results can be found online at <https://github.com/jtxiao/Vertical-PV-on-Tower-HOMER-Results>.

#### The Impact of the Fuel Efficiency Curve

For the most part, these results are intuitive. As grid reliability goes up, the need for PV and external power sources trends down. Similarly, as PV cost increases, the demand for solar decreases. However, there appear to be some discrepancies. For example, when PV costs \$2.6/W, PV is favorable for reliabilities of 4 hours per day, but not 0.

This discrepancy actually comes from the diesel generator fuel efficiency. As the generator runs at higher loads, it uses fuel more efficiently, wasting less energy. For the worst grid reliabilities, the power demand on the generators becomes higher so its load increases, using fuel more efficiently. This saves a nontrivial amount of diesel opex, making PV less attractive.

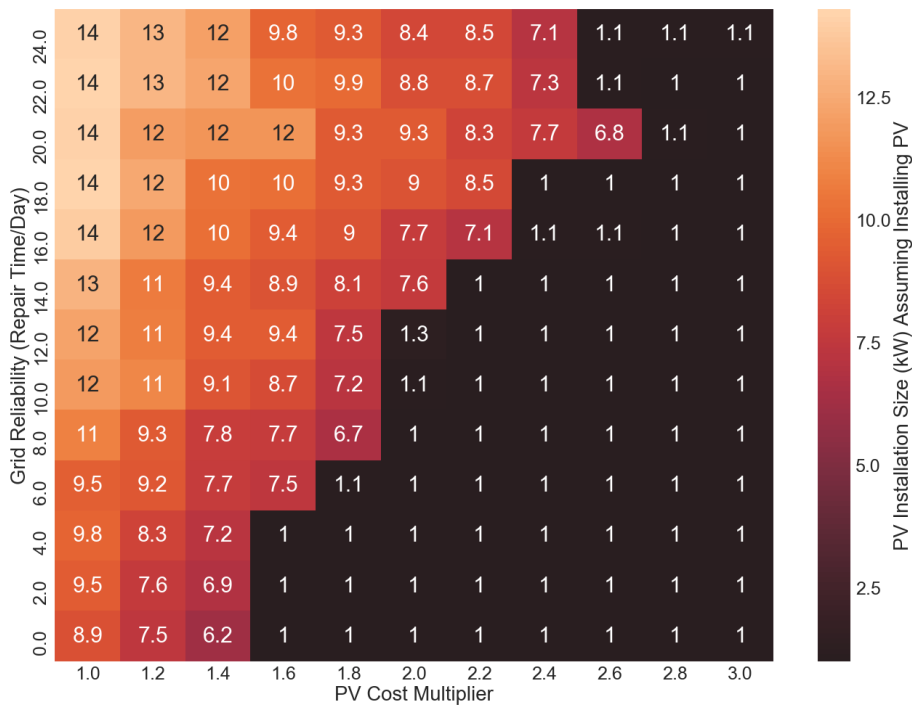


Figure 3-8: Heat map of optimal PV installation size (1 kWp minimum) with varying PV cost and grid reliability in Rajasthan, India.

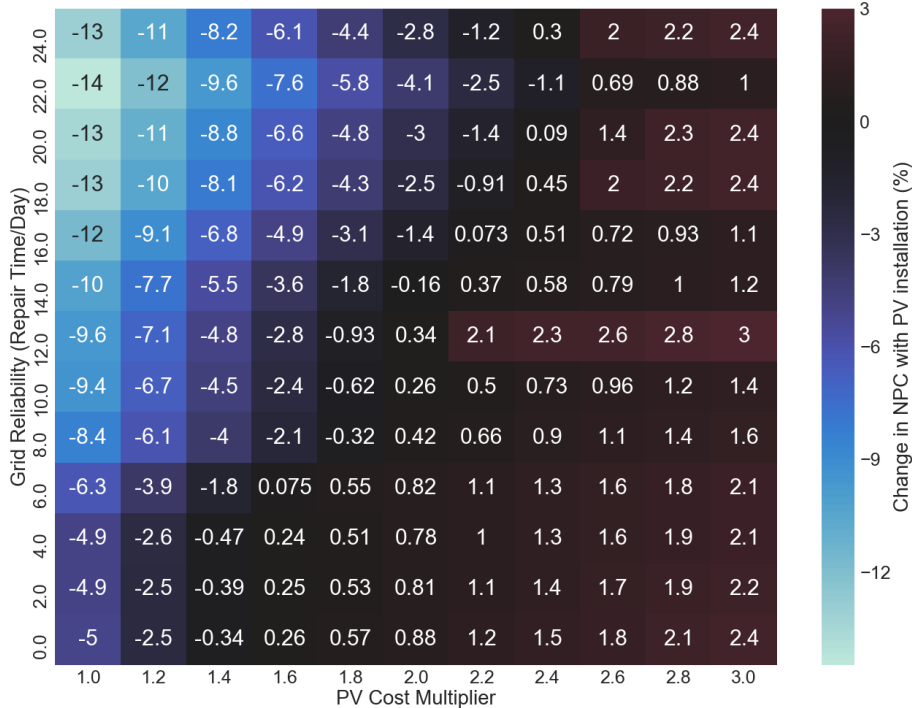


Figure 3-9: Heat map of change in net present cost given the PV installation in Figure 3-8 with varying PV cost and grid reliability in Rajasthan, India.

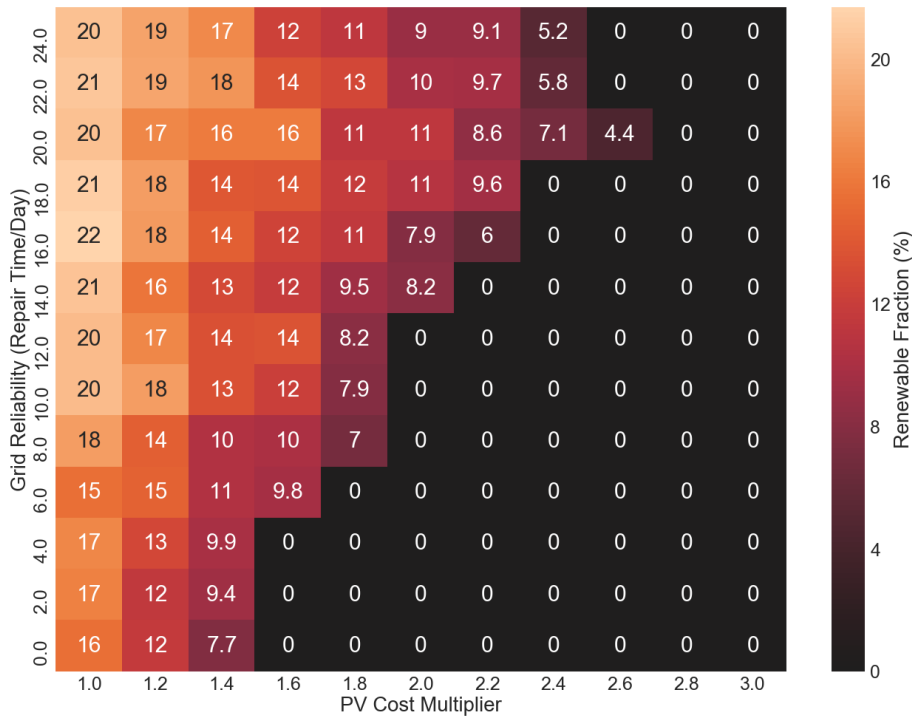


Figure 3-10: Heat map of renewable fraction given the PV installation in Figure 3-8 with varying PV cost and grid reliability in Rajasthan, India.

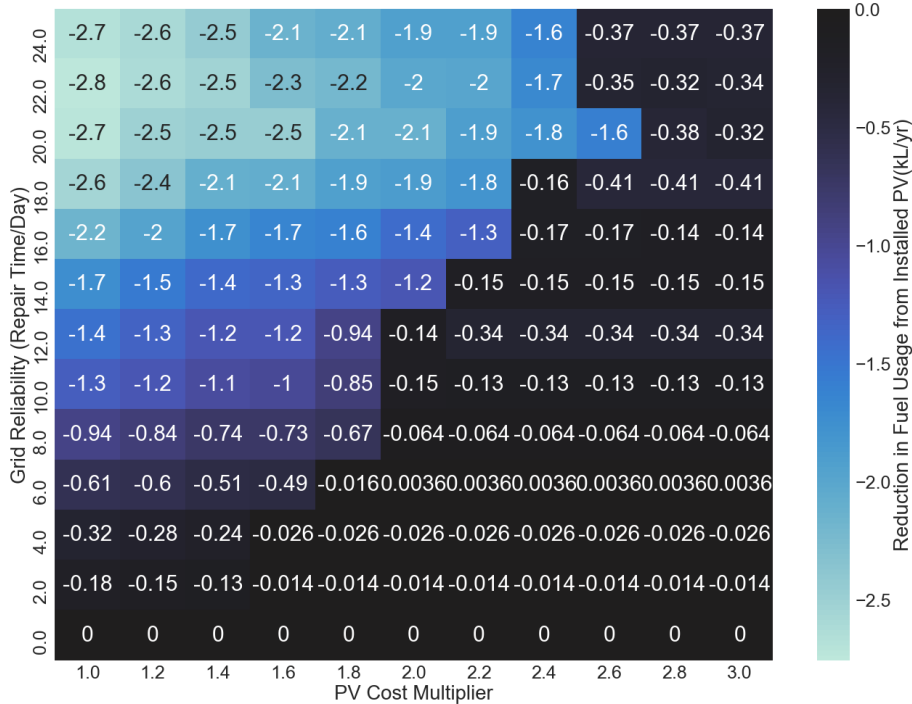


Figure 3-11: Heat map of change in diesel usage given the PV installation in Figure 3-8 with varying PV cost and grid reliability in Rajasthan, India.

For example, let's look at the case for \$2.4/W PV cost and 0 hours of grid reliability. Optimally, the system wants to install no PV; in that case it consumes 8,974 L/yr of fuel and produces 41,688 kWh/yr, with a total NPC of \$108,193. This comes out to \$0.21967/kWh. On the other hand, if we force the system to install 7.1 kWp of PV, because of the lower load on the generator it consumes 7,348 L/yr of fuel to produce 33,628 kWh/yr of energy. This translates to a diesel cost of energy of \$0.22287/kWh, which accumulates over the 10 years to a total diesel cost of \$73480. The system now has an NPC of \$108,514, which is a \$321 increase. If the generator had a linear efficiency curve, such that its \$/kWh cost is the same at all loads, then the total diesel cost for the 7.1 kWp PV case would be  $\$0.21967/\text{kWh} \times 336\,258 \text{ kWh} \times 10 \text{ yr} = \$73090$ . We see that the difference in price from diesel efficiency alone comes out to \$390, which accounts for the \$321 increase in price from installing PV.

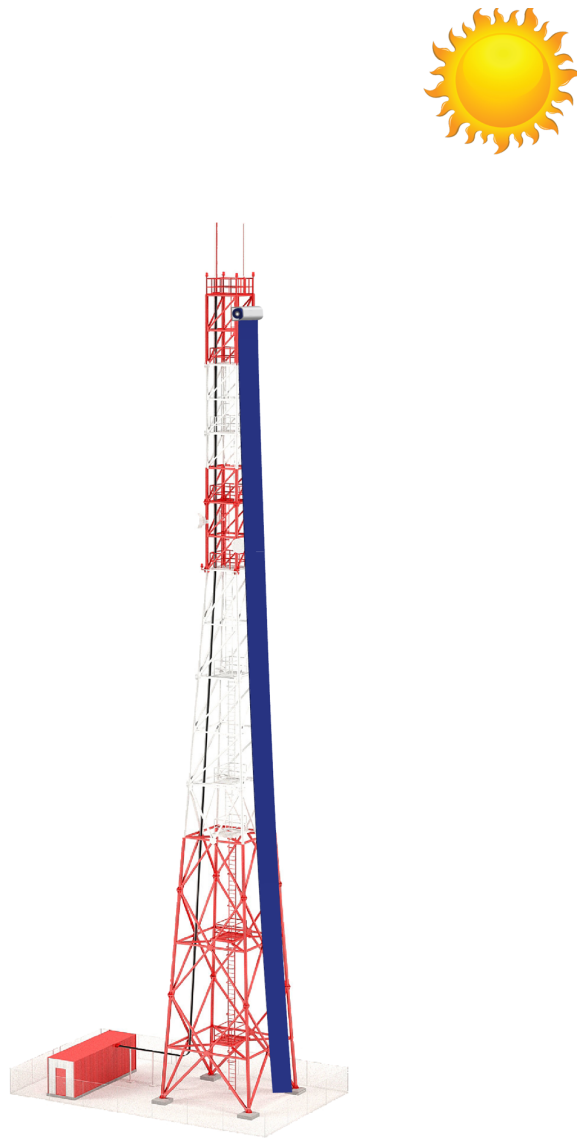
### 3.5.2 Is Vertical PV Financially Viable in India?

There are many areas of India with grid reliabilities of less than 12 hours a day. It is very promising, then, that given the predicted price range of \$1.5/W - \$2/W for perovskite PV, it is financially favorable to install PV for grid reliabilities of up to around 10 hours per day, and for PV costs between \$1.5/W - \$1.8/W we are encouraged to install PV for reliabilities up to around 16 hours a day. As India rapidly works to improve its grid, these higher numbers for reliability are becoming more widespread. It's encouraging that these results remain robust for better grid connection.

Encouraging, also, is the green impact that the PV installation serves. Installing such a large amount of PV leads to around 10-15% renewable fraction (ignoring the amount stored in the battery), and an annual reduction in fuel usage of 1000 - 2500 kL. This translates to approximately 2.7 - 6.75 less tons of CO<sub>2</sub> per year per tower. From both a cost and environmental benefit, we predict that installing vertical perovskite PV on communications towers in India makes sense.

### 3.6 Chapter Acknowledgements

Ryan Zimmerman provided wind load calculations and performed FEA simulations on wind loading. ATC provided data on telecommunications towers and funded this work.





# Chapter 4

## Conclusions and Future Work

In this work we have developed a Monte Carlo cost modeling method and applied it to a realistic perovskite manufacturing sequence. Because of the extremely cheap cost of the active materials, we found a cost-competitive price range. With obvious cost component targets, we proposed possible pathways to bring this price down even further.

We applied our cost model results to see if a real world application of powering telecommunications towers with vertically mounted perovskite PV makes financial sense. We first ensured that a large amount of PV could be mounted without creating structural failure modes through wind load. This gave an upper bound on PV size, which informed our economic analysis. Using HOMER, we analyzed the financial feasibility of vertically mounted PV in Nigeria and India. We found that at the current low diesel price in Nigeria, it is not cost-effective to use vertical PV. However, with the global increasing of diesel prices, it may very well become feasible. In India, with its high variance in grid reliability, we determined that vertical PV is cheaper and greener for areas with grid reliabilities as high as 16 hours a day. Thus, there exists a potential market application for perovskite PV.

In continuing partnership with ATC, we would like to further our studies by investigating possible deployment solutions for vertically mounted PV on towers. We would like to develop high-speed, automated, and cost-effective methods for primarily vertically mounted PV, but also commercial rooftop and utility-scale PV. As the study

continues, cost parameters will likely change. We will thus regularly update the cost model to account for more refined and updated inputs.

With all of this in mind, we strongly believe in the potential of perovskite solar. Though perovskite PV is not without its faults (stability issues and possible toxicity from lead), these issues are continually being researched and mitigated. Its low cost and high efficiency, combined with its potential lightweight and flexible form factor, make perovskite PV a promising technology for making the world a greener place.

# Appendix A

## Cost Model Inputs

### A.1 Materials Inputs

Presented in Table A.1 is the list of all materials inputs and their nominal, low, and high estimates for usage and cost. Values are either taken from discussion with Dirk Weiss, Nathan Chang, Sarah Sofia, Tomas Leijtens, Max Hoerantner, and the GridEdge/ONE Lab team, or from References [7] and [24]. Usage is in units/m<sup>2</sup>, while cost is in \$/units.

Process	Material	Nominal Usage	Nominal Cost	Low Usage	Low Cost	High Usage	High Cost	Unit
PET Receipt	PET	1	2	1	1	1	4	m <sup>2</sup>
IZO sputter	IZO	1.405	0.324	0.702	0.02	2.107	0.898	g
NiOx sputter	NiOx	0.1	1.979	0.033	0.249	0.2	4.233	g
FACsPbIBr slot die	CsBr	0.134	0.26	0.108	0.031	0.269	0.568	g
	FaBr	0.385	0.584	0.308	0.087	0.77	1.176	g
	PbI <sub>2</sub>	1.284	0.078	1.028	0.003	2.569	0.263	g
	PbBr <sub>2</sub>	0.341	0.157	0.273	0.024	0.682	0.311	g
PCBM slot die	PCBM	0.068	24.12	0.068	1.144	0.068	73.891	g
	Anisole	3.4	0.013	3.4	0.004	3.4	0.02	mL
SnO <sub>2</sub> sputter	SnO <sub>2</sub>	0.07	1.513	0.035	0.224	0.139	3.051	g
Al sputter	Al	0.27	0.267	0.135	0.029	0.81	0.605	g
Encapsulate	Barrier films	2	20	2	5	2	40	m <sup>2</sup>
	Adhesive	3	0.164	2.5	0.074	3.5	0.351	g
Cut and contact	Contact buttons	13.1	0.1	13.1	0.05	13.1	0.2	pair
J-box install	Junction box	1	8.5	0.5	5	2	12	m <sup>2</sup>

Table A.1: Cost model materials inputs

## A.2 Tools Inputs

Presented in Table A.2 and A.3 are the lists of all tools input estimates, in the format nominal (low - high). Values are either taken from discussion or from References [7],[25], and [24].

Process	Tool	Tool cost	Facility cost	Floor space	Spare parts	Electricity usage
Web clean	Web cleaner	0.029 (0.022-0.037)	2 (1-3)	5 (4-8)	3 (2-4)	10 (5-20)
IZO/NiOx/SnO <sub>2</sub> sputter	Sputterer	6.5625 (5.25-7.875)	25 (20-30)	25 (20-30)	4 (3.2-4.8)	500 (400-600)
P1/P2/P3 scribe	Laser scribe	0.8 (0.64-0.96)	25 (20-30)	15 (12-18)	4 (3.2-4.8)	2 (1.6-2.4)
NiOx/FACsPbIBr flash anneal	Flash annealer	0.25 (0.2-1)	25 (20-30)	10 (5-20)	3 (2-4)	100 (50-200)
FACsPbIBr/PCBM slot die	Slot die coater	0.632(0.441-0.864)	30 (20-40)	30 (20-40)	10 (5-20)	40 (20-60)
Al sputter	Sputterer	6.5625 (5.25-7.875)	25 (20-30)	12.5 (10-15)	4 (3.2-4.8)	80 (64-96)
Encapsulate	Laminator	1.958 (1.566-2.349)	25 (20-30)	15 (12-18)	4 (3.2-4.8)	35 (28-42)
Cut and contact	Sheet and pin tool	0.029 (0.022-0.037)	2 (1-3)	5 (4-8)	4 (2-8)	10 (5-20)
J-box install	J-box tool	0.504 (0.404-0.605)	25 (20-30)	2.5 (2-3)	4 (3.2-4.8)	0.5 (0.4-0.6)
Module test	Module tester	1.656 (1.325-1.988)	25 (20-30)	2.5 (2-3)	4 (3.2-4.8)	0.5 (0.4-0.6)

Table A.2: Tool cost inputs, where tool cost (\$M) is the total upfront cost of the tool, facility cost (% of tool cost) is the cost of support services such as air or chemical delivery, floor space (m<sup>2</sup>) is the footprint of the tool itself, spare parts (% capex/yr) is any replacement parts that the tool needs every year, and electricity usage (kW) is the power demand of the tool.

Process	Tool	Throughput	Downtime	Operation staff	Maintenance staff	Yield
Web clean	Web cleaner	4 (3-5)	2 (1-3)	0.02 (0.01-0.04)	2 (1-3)	99.5 (99-100)
IZO/NiOx/SnO <sub>2</sub> sputter	Sputterer	67.2 (53.76-80.64)	3 (2-5)	0.25 (0.2-0.5)	2 (1-3)	98 (96-100)
P1/P2/P3 scribe	Laser scribe	52 (41.6-62.4)	2 (1-3)	0.25 (0.2-0.5)	2 (1-3)	99.5 (98-100)
NiOx/FACsPbIBr flash anneal	Flash annealer	100 (80-120)	2 (1-10)	0.25 (0.2-0.5)	2 (1-3)	99 (98-100)
FACsPbIBr/PCBM slot die	Slot die coater	18(18-18)	10 (5-20)	0.5 (0.25-1)	2 (1-3)	98 (96-100)
Al sputter	Sputterer	67.2 (53.76-80.64)	3 (2-5)	0.25 (0.2-0.5)	2 (1-3)	98 (96-100)
Encapsulate	Laminator	67.2 (53.76-80.64)	2 (1-5)	0.02 (0.01-0.04)	2 (1-3)	99.5 (99-100)
Cut and contact	Sheet and pin tool	4 (3-5)	2 (1-3)	0.02 (0.01-0.04)	2 (1-3)	99.5 (99-100)
J-box install	J-box tool	67.2 (53.76-80.64)	2 (1-3)	0.02 (0.01-0.04)	2 (1-3)	99.5 (99-100)
Module test	Module tester	67.2 (53.76-80.64)	5 (3-8)	0.02 (0.01-0.04)	2 (1-3)	99.5 (99-100)

Table A.3: Tool cost inputs, where throughput is the area process in an hour of operation (m<sup>2</sup>/hr), downtime is the percentage of time the tool is maintained instead of operating (% of time), operation staff is the number of operators needed to operate the tool, maintenance staff is the number of staff needed to conduct maintenance or repair, and yield is the percentage of modules process that are good (%).

## A.3 Factory Assumptions

Presented in Table A.4 is the list of all factory assumptions and their nominal, low, and high estimates. Values are either taken from discussion or from Reference [7].

<i>Factory assumption</i>	<i>Nominal estimate</i>	<i>Low estimate</i>	<i>High estimate</i>
Electricity cost (\$/kWh)	0.11	0.07	0.13
Electricity for services	1	1	1
Floor space ratio	3	2	5
Building cost (\$/m <sup>2</sup> )	1000	200	1500
Operator labor rate (\$/hr)	20	15	30
Maintenance technician labor rate	25	20	30
Indirect labor cost ratio	0	0	0
Facilities depreciation time	15	15	15
Equipment depreciation time	7	7	7
Number of operating hours	3690	2630	6130

Table A.4: Factory assumptions, where the electricity cost is the local cost of grid electricity, electricity for services is the ratio of electricity for services/tool electricity, floor space ratio is the ratio of total factory floor space/tool footprint, building cost is the cost of building a factory, operator labor rate is the wage for operators, maintenance technician labor rate is the technician wage, indirect labor cost ratio is the ratio of indirect labor/direct labor (set to 0 here because it is accounted for in later steps), facilities and equipment depreciation times are the depreciation times for all facilities and tools respectively, and number of operating hours is the hours per year the factory operates.



# Bibliography

- [1] Structural standard for antenna supporting structures and antennas. *TIA Standard*, August 2015.
- [2] Homer® Pro Version 3.7 User Manual, August 2016.
- [3] Diesel prices, liter. [https://www.globalpetrolprices.com/Nigeria/diesel\\_prices/](https://www.globalpetrolprices.com/Nigeria/diesel_prices/), May 2018.
- [4] U.S Energy Information Administration. How much carbon dioxide is produced from burning gasoline and diesel fuel? <https://www.eia.gov/tools/faqs/faq.php?id=307&t=11>, May 2017.
- [5] International Energy Agency. *Renewables 2017*, October 2017.
- [6] Pew Research Center. March 2016 political survey, March 2016.
- [7] Nathan L. Chang, Anita Wing Yi Ho-Baillie, Doojin Vak, Mei Gao, Martin A. Green, and Renate J. Egan. Manufacturing cost and market potential analysis of demonstrated roll-to-roll perovskite photovoltaic cell processes. *Solar Energy Materials and Solar Cells*, 174:314 – 324, 2018.
- [8] Nathan L. Chang, Anita Wing Yi Ho-Baillie, Paul A. Basore, Trevor L. Young, Rhett Evans, and Renate J. Egan. A manufacturing cost estimation method with uncertainty analysis and its application to perovskite on glass photovoltaic modules. *Progress in Photovoltaics: Research and Applications*, 25(5):390–405.
- [9] Valerio D’Innocenzo, Giulia Grancini, Marcelo J. P. Alcocer, Ajay Ram Srimath Kandada, Samuel D. Stranks, Michael M. Lee, Guglielmo Lanzani, Henry J. Snaith, and Annamaria Petrozza. Excitons versus free charges in organo-lead tri-halide perovskites. *Nature Communications*, 5:3586, Apr 2014.
- [10] Christopher Eames, Jarvist M. Frost, Piers R. F. Barnes, Brian C. O’Regan, Aron Walsh, and M. Saiful Islam. Ionic transport in hybrid lead iodide perovskite solar cells. *Nature Communications*, 6:7497, Jun 2015.
- [11] Michael Forsyth. China aims to spend at least \$360 billion on renewable energy by 2020. *The New York Times*, January 2017.

- [12] Manish Kumar Hairat and Sajal Ghosh. 100GW solar power in india by 2022 – a critical review. *Renewable and Sustainable Energy Reviews*, 73:1041 – 1050, 2017.
- [13] David Hulett. *Integrated Cost-Schedule Risk Analysis*. Goer Publishing, Ltd, 9 2012.
- [14] Fraunhofer ISE. Photovoltaics Report, July 2014.
- [15] Tomas Leijtens, Kevin Bush, Rongrong Cheacharoen, Rachel Beal, Andrea Bowring, and Michael D. McGehee. Towards enabling stable lead halide perovskite solar cells; interplay between structural, environmental, and thermal stability. *J. Mater. Chem. A*, 5:11483–11500, 2017.
- [16] Saliba Michael, Correa-Baena Juan-Pablo, Grätzel Michael, Hagfeldt Anders, and Abate Antonio. Perovskite solar cells: From the atomic level to film quality and device performance. *Angewandte Chemie International Edition*, 57(10):2554–2569.
- [17] Sylke V. Schnepf Milena Buchs. Uk households' carbon footprint: A comparison of the association between household characteristics and emissions from home energy, transport and other goods and services. *Discussion Paper Series*, May 2013.
- [18] D. M. Powell, M. T. Winkler, H. J. Choi, C. B. Simmons, D. Berney Needleman, and T. Buonassisi. Crystalline silicon photovoltaics: a cost analysis framework for determining technology pathways to reach baseload electricity costs. *Energy Environ. Sci.*, 5:5874–5883, 2012.
- [19] Robert Margolis Mike Woodhouse Ran Fu, David Feldman and Kristen Ardani. U.S. solar photovoltaic system cost benchmark: Q1 2017. 2016.
- [20] Stefano Razza, Sergio Castro-Hermosa, Aldo Di Carlo, and Thomas M. Brown. Research update: Large-area deposition, coating, printing, and processing techniques for the upscaling of perovskite solar cell technology. *APL Materials*, 4(9):091508, 2016.
- [21] William Shockley and Hans J. Quiesser. Detailed balance limit of efficiency of p-n junction solar cells. *Journal of Applied Physics*, 32:510, 1961.
- [22] Collavini Silvia, Völker F. Sebastian, and Delgado Juan Luis. Understanding the outstanding power conversion efficiency of perovskite-based solar cells. *Angewandte Chemie International Edition*, 54(34):9757–9759.
- [23] Rajesh Kumar Singh and Saket Sundria. Living in the dark: 240 million indians have no electricity. *Bloomberg*, Jan 2017.

- [24] Sarah E. Sofia, Jonathan P. Mailoa, Dirk N. Weiss, Billy J. Stanbery, Tonio Buonassisi, and I. Marius Peters. Economic viability of thin-film tandem solar modules in the united states. *Nature Energy*, 3(5):387–394, 2018.
- [25] Zhaoning Song, Chad L. McElvany, Adam B. Phillips, Ilke Celik, Patrick W. Krantz, Suneth C. Watthage, Geethika K. Liyanage, Defne Apul, and Michael J. Heben. A technoeconomic analysis of perovskite solar module manufacturing with low-cost materials and techniques. *Energy Environ. Sci.*, 10:1297–1305, 2017.
- [26] Nidhi Verma. India’s oil imports hit record high in january - trade. *Reuters*, Feb 2018.
- [27] L. Wang, G. D. Yuan, R. F. Duan, F. Huang, T. B. Wei, Z. Q. Liu, J. X. Wang, and J. M. Li. Tunable bandgap in hybrid perovskite CH<sub>3</sub>NH<sub>3</sub>Pb(Br<sub>3</sub>yX<sub>y</sub>) single crystals and photodetector applications. *AIP Advances*, 6(4):045115, 2016.
- [28] Wan-Jian Yin, Tingting Shi, and Yanfa Yan. Unusual defect physics in CH<sub>3</sub>NH<sub>3</sub>PbI<sub>3</sub> perovskite solar cell absorber. *Applied Physics Letters*, 104(6):063903, 2014.
- [29] Kunta Yoshikawa, Hayato Kawasaki, Wataru Yoshida, Toru Irie, Katsunori Konishi, Kunihiro Nakano, Toshihiko Uto, Daisuke Adachi, Masanori Kanematsu, Hisashi Uzu, and Kenji Yamamoto. Silicon heterojunction solar cell with interdigitated back contacts for a photoconversion efficiency over 26%. *Nature Energy*, 2:17032 EP –, Mar 2017. Article.